THE ROLE OF MICROSTRUCTURE IN THE OXIDATION OF THE Mo-Ni-Al SYSTEM

by

Jose Yebrail Diaz

T 1331

A thesis submitted to the Faculty and the Board of Trustees of Colorado School of Mines in partial fulfillment of the requirements of the degree of Master of Science in Metallurgical Engineering.

Signed: J. Y. Diaz
Jose Yebrail Diaz

Golden, Colorado
Date: Nov. 30, 1970

Approved: W D Copeland
William D. Copeland
Thesis Advisor

Paul G. Herold
Paul G. Herold
Head of Department
Metallurgical Engineering

Golden, Colorado
Date: Nov. 30, 1970

T 1331

ABSTRACT

Oxidation tests were performed on some alloys of the system Al-Mo-Ni. The nickel composition was chosen around the intermetallic compound NiAl and molybdenum was added up to 60% by weight. Resistance to oxidation at high temperature was a function of composition, temperature, and microstructure. Mo_3Al was found by x-ray analysis in alloys with molybdenum content above 3%. An increase in melting point was observed in alloy with Ni/Al of 1.0 and 1.5 as molybdenum was added.

CONTENTS

LIST OF FIGURES

ACKNOWLEDGMENTS

The author wishes to gratefully acknowledge the guidance and advice given by Dr. William D. Copeland, Professor of Metallurgy, who served as graduate advisor for this work. The author also wishes to thank Dr. N. Cyril Schieltz for his guidance in x-ray analysis. Thanks are also expressed to Colorado School of Mines Foundation for providing financial support to the author for the duration of this study.

INTRODUCTION

Although numerous studies on the oxidation of metals and alloys have been reported in the current literature, little is known about the reaction mechanisms. This is due mainly to a present lack in knowledge of important aspects such as phase diagrams and structures of some oxides and metallic systems, diffusion data at high temperature, state of stresses in oxide scales, and adsorption phenomena on metallic surfaces. Up to now, the most significant approach to the problem has been the Wagner-Schottly-Hauffe semiconductor valence theory but, unfortunately, it can be applied successfully only when certain conditions are satisfied (Hauffe, K., 1965, p. 170).

The molybdenum alloys have not been well studied because of their tendency toward catastrophic oxidation at low temperatures due to the formation of MoO_3 which has a melting point of only 726°C; nevertheless, Zitzer, D., (1964, p. 86) describes a process whereby NiAl compound covered molybdenum at high temperatures and a NiAl-Mo bond inhibited catastrophic oxidation. Based on the former results, oxidation tests were performed on alloys with different percentages of nickel, aluminum and molybdenum to see the effect of composition and also on pre-heat treated samples to see the effect of the microstructure in the oxidation resistance at high temperature (1200°C).

In order to learn how oxidation proceeds in these alloys, it is the author's opinion that it is necessary to find out:

a) the mechanisms in adsorption at high temperature and variable oxygen pressure.

b) the components and products in the reaction of oxidation when temperature, pressure, and time are the variables for a given composition.

c) the structural defects in oxides and their effects on electrical conductivity, diffusion and oxidation rates.

Some conclusions were obtained in this research, but it is expected that a future work will explain more completely the oxidation in molybdenum-nickel-aluminum ternary alloys.

THEORY AND LITERATURE SURVEY

Oxygen Adsorption and Initial Oxidation

The adsorption of oxygen is an exothermic process by which the surface free energy is decreased (irreversible process) and the ordering of oxygen atoms on the metallic surface is increased. If an activation energy is associated, the adsorption becomes a determining parameter in the initial part of the oxidation at high temperature.

Studies on nickel surfaces based on flash desorption field emission microscopy and low-electron diffraction techniques have discovered that adsorption rate depends on the crystallographic orientation and surface defects, proceeding until a monolayer of the absorbed element is formed on the metallic surface (Kofstad, P., 1966, p. 23). Once the monolayer has been formed, oxidation begins by heterogeneous nucleation on preferred sites where a possible decrease in free energy can occur. The sites where imperfections like dislocations, Frenkel or Schottky defects, precipitated particles, phase boundaries, concentration gradients, etc. are located, have a larger internal energy (negative) as compared with perfect crystals, and it is believed that they will be the preferred sites for initial oxidation. If this is so, a pure metal will be more resistant to oxidation than an alloy, an annealed metal more than a cold worked metal, and a solid solution more than a

supersaturated solid solution when a second phase precipitates along grain boundaries. Farnsworth, H., and Tual, J., (1958, p. 48) reported that after nucleation, a directional growth of individual crystallites proceeds according to the existing conditions of temperature, surrounding atmosphere and surface.

During initial oxide formation, adsorption is often rate determining, the extent of this phase depending on the oxygen pressure, the temperature, and the nature of the oxide already formed (Kofstad, P., 1966, p. 237).

When the solubility of oxygen in the metal or alloy is large, diffusion instead of adsorption is the rate-determining factor in initial oxidation. The solubility of oxygen in Ni-Al-Mo alloys even at high temperature as 1200°C is still very low to be an important factor, but instead the volatilization of MoO_3 when formed is thought to be the rate determining factor in most molybdenum alloys. When this occurs a nearly linear oxidation rate prevails and the alloy cannot be used at high temperature.

Thermodynamics and Kinetics in Oxidation

Although an oxidation reaction may be thermodynamically possible, it may occur very slowly when the attainment of the equilibrium is impeded by a low rate of reaction. The rate of reaction which is given by the Arrhenius equation:

$$b = Ae^{-Q/RT}$$

where

Q = activation energy for the oxidation reaction

R = gas constant

T = absolute temperature

A = constant for each particular reaction

will depend on the respective coefficients of diffusion of metal and oxygen inside the oxide. In the most general case, these coefficients of diffusion do not have the same numerical value and a concentration of metal or oxygen vacancies is formed, resulting in a non-stoichiometric oxide.

As electrons have to be left by the metal at the metal/oxide boundary and taken by the adsorbed oxygen at the oxygen/oxide boundary, electrical conductivity of the oxide layer plays an important role in the rate of ionization which is the previous step in oxide formation as is observed in Figure 1. The following general reactions are thought to take place in oxidation phenomenon:

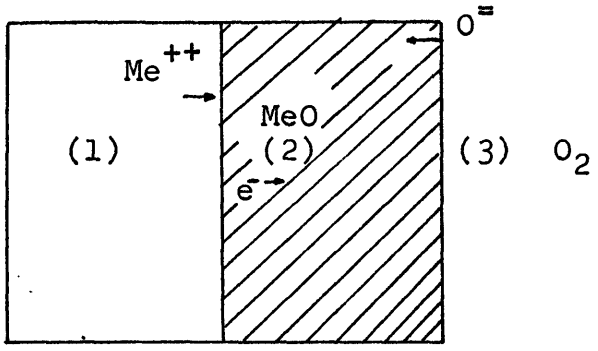

Reaction at oxygen/oxide boundary: $\frac{1}{2}O_2 + 2e^- \rightarrow O^=$

Reaction at metal/oxide boundary: $Me - 2e^- \rightarrow Me^{++}$

Oxidation reaction: $\frac{1}{2}\ O_2 + Me \rightarrow Me^{++} + O^=$ (ionic)

Figure 1. The oxidation reactions of a metal through a protective oxide layer.

(1) $M - 2e^- \rightarrow M^{++}$ oxidation of metal — ionization reactions

$\frac{1}{2}O_2 + 2e^- \rightarrow \frac{1}{2}O_2^=$ reduction of oxygen

(2) $M^{++} + \frac{1}{2}O_2^= \rightarrow$ ionic oxide

The first two reactions depend on electrical conductivity and the last on diffusivity.

There are four types of oxidation behavior depending on thermodynamic and kinetic properties of the oxides (Albeit, 1960, p. 383).

1) Linear behavior: when a protective oxide is absent and the oxidation equation is $W = At$

where:

A = constant that depends on temperature

W = increase or decrease in weight

t = time

This behavior is also called non-kinetic because the metal-

oxygen contact is direct and there is no necessity for diffusion for the oxide to be formed. This is the case of volatilized, porous, or cracked oxides.

2) Parabolic behavior: when there is a protective oxide growing according to the steady-state Fick's equation:

$$W^2 = At$$

The driving force for oxidation will be the concentration gradient between the metal at the metal/oxide boundary and the metal at the oxide/oxygen boundary, and the thickness of the oxide layer increases as the square root of the time of oxidation.

3) Logarithmic behavior: when there is a protective oxide growing according to the second Fick's law. This is the most common case for pure metals. The rate of oxidation is a function of time as the metal concentration at the oxide/oxygen boundary is not a constant.

4) Mixed behavior: when there is a protective or non-protective oxide which does not follow any definite behavior, but is changing continuously. This is the most common case in alloys.

These behaviors are explained in Figure 2.

According to the internal structure of the oxides, the oxidation rate will depend on the electrical conductivity which is a function of the kind of defects present in it. If the oxide is stoichiometric, with Shottky or Frenkel disorder, the conductivity is considered low because it is

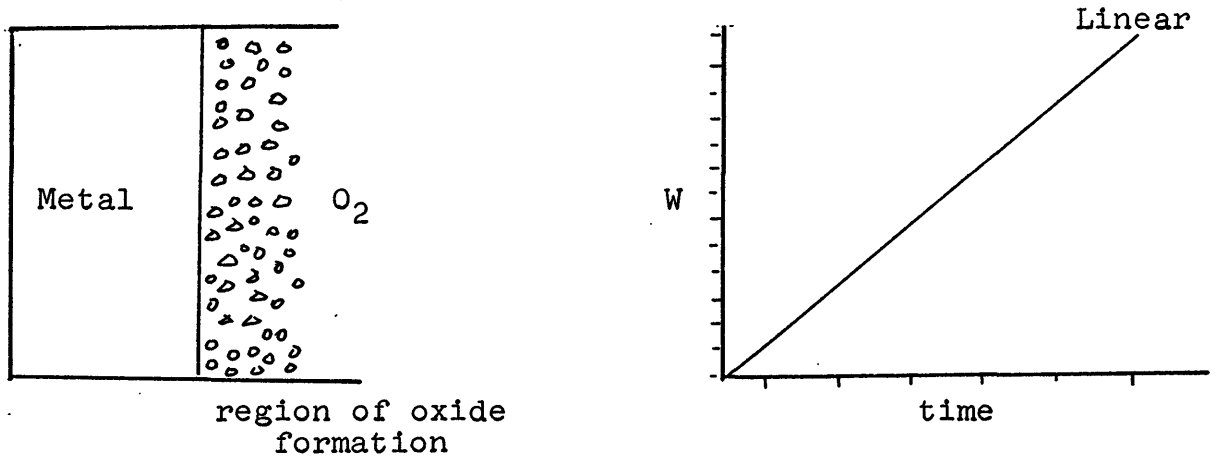

a) The oxide film is porous and molecular oxygen can pass into its pores and react at the metal-oxide interface.

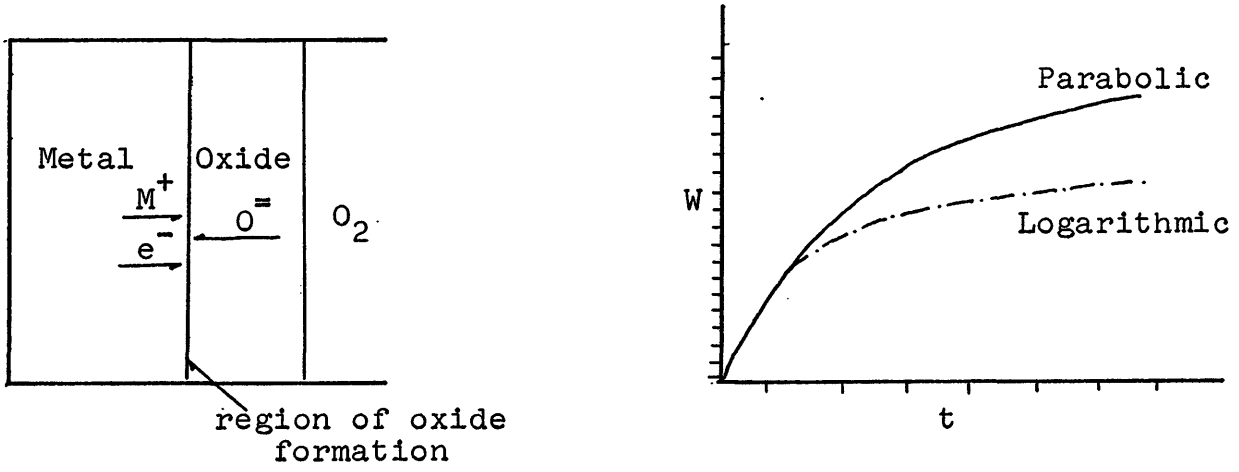

b) The oxide film is protective and oxygen diffusivity is higher than metal diffusivity.

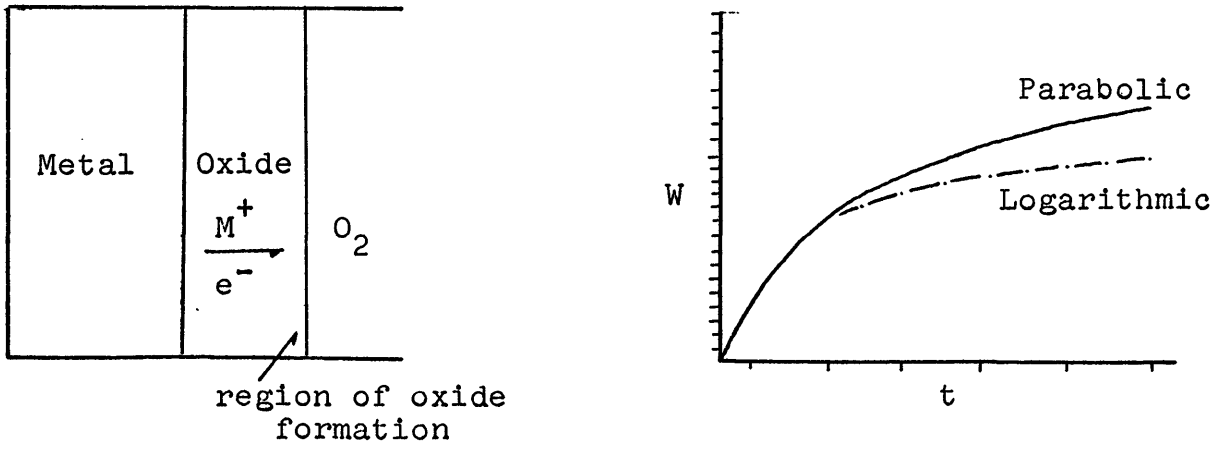

c) The oxide film is protective and oxygen diffusivity is lower than metal diffusivity.

Figure 2. Protective and non-protective oxides.

ionic, but the most common case is when these defects interact and associate with each other or with impurities atoms, giving more complex defects, i.e. non-stoichiometric oxides of the cation or anion defect type, and in order to conserve the electrical neutrality, additional electrons or holes are simultaneously created (n, p semiconductors). The effect of foreign impurities atoms on oxidation rates in non-stoichiometric oxides is:

1) Metal excess oxide (M_{b+n} O). The metal excess goes to interstitial positions and the electrical conductivity is increased because there is an excess of conduction electrons when the ionization reaction takes place:

$$M \rightarrow M^{n+} + ne^{-}$$

where

M = metal excess

M^{n+} = interstitial metal

ne^{-} = conduction electrons

Further increase in conductivity is obtained with additions of higher valence cations, and decrease by increasing oxygen pressure.

2) Metal deficit oxide (M_{b-n} O). The metal deficit is produced by metal vacancies and electrons holes are simultaneously created in order to conserve the electrical neutrality when the following reaction takes place:

$$M = V_{ne}^{n-} + ne^{+}$$

where

M = metal deficit

V_{ne}^{n-} = metal vacancies

ne^{+} = conduction electrons holes

Further increase in conductivity is obtained by increasing the oxygen pressure and decrease is obtained with additions of higher valency cations.

3) Oxygen excess oxide (MO_{a+y}). The oxygen excess goes to interstitial positions and electrons holes are simultaneously created in order to conserve the electrical neutrality when the following reaction takes place

$$O = O_i^{=} + 2e^{+}$$

where

O = oxygen excess

$O_i^{=}$ = oxygen interstitial

e^{+} = conduction electrons holes

Further increase in conductivity is obtained by increasing the oxygen pressure and decrease is obtained with additions of higher valency cations.

4) Oxygen deficit oxide (MO_{o-x}). The oxygen defect is as oxygen vacancies, and electrons are simultaneously created in order to conserve the electrical neutrality when the following reaction takes place

$$O = Vo^{++} + 2e^{-}$$

where

O = oxygen deficit

Vo^{++} = oxygen vacancies

e^- = conduction electrons

Further increase in conductivity is obtained with additions of higher valency cations and decrease is obtained by increasing the oxygen pressure.

The next section of the literature survey was directed toward searching for data on the theoretically existing oxides at high temperatures: NiO, Al_2O_3, MoO_3, and MoO_3. Figure 3 shows the thermodynamic possibilities for nickel, aluminum, and molybdenum oxide formation as a function of temperature.

Nickel Oxide (NiO) - It is a metal deficit oxide whose electrical conductivity is given by the equation (Kubaschewsky, 1953, p. 31)

$$\sigma = Ae^{-Q/RT} = B(P_{O_2})^{1/8}$$

where

σ = electrical conductivity which is directly proportional to the rate of reaction

Q = activation energy

A,B = constants

P_{O_2} = oxygen pressure

The excess of oxygen by effect of a high oxygen pressure creates nickel vacancies and the electroneutrality is

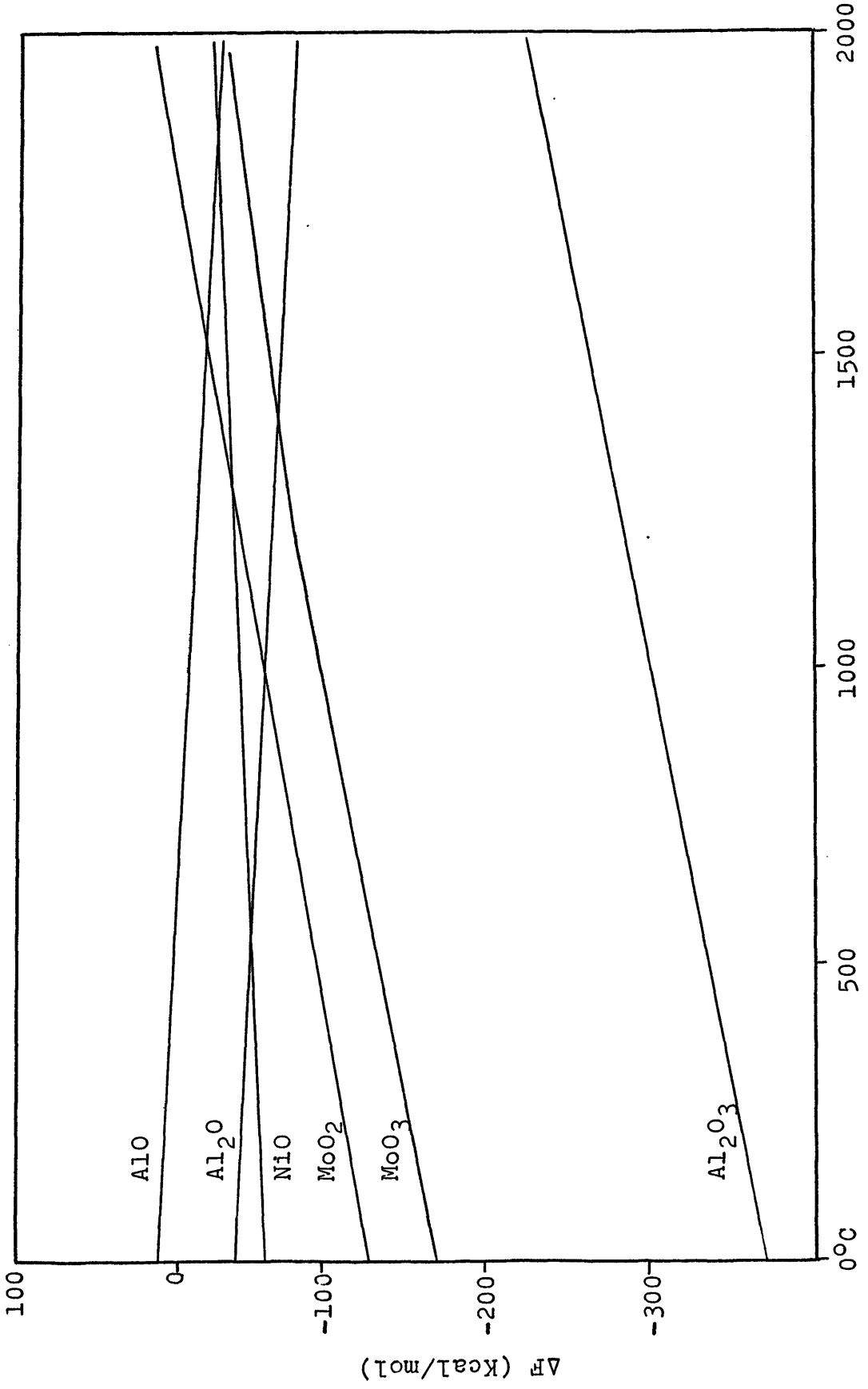

Figure 3. The standard free energy of formation of the oxides in Al-Ni-Mo system as a function of temperature (Vicks, C., and Block, F., 1963).

achieved by electron holes which are responsible for the increments in rates of oxidation. At high temperature these increments in rates of oxidation are due to the creation of nickel vacancies according to the equation

$$N_v = e^{-Q_f/RT}$$

where

N_v = ratio of vacancies to atoms

Q_f = activation energy per mol of vacancies

T = temperature

The electrical conductivity in NiO can be explained in two ways as shown in figures 4 and 5. In the first case the conductivity is caused by an exchange of valence between bivalent and trivalent nickel ions which are considered as mobile valence states. The defect reaction in this case is:

$$N_i + \tfrac{1}{2}O_2 \rightleftarrows V^{o}_{Ni} + NiO$$

where

V^{o}_{Ni} = neutral vacancy

NiO = ionic oxide with trivalent and bivalent nickel ions

The conductivity is thought to be due to a rapid exchange of valence between trivalent and bivalent nickel ions. In the second case, the conductivity occurs by a free movement of electron holes inside the oxide. The defect reaction in this case is:

$$Ni + \tfrac{1}{2}O_2 \rightleftarrows V^{=}_{Ni} + 2e^{+} + NiO$$

$O^{=}$	Ni^{++}	$O^{=}$	Ni^{+++}	$O^{=}$
Ni^{++}	$O^{=}$	Ni^{++}	$O^{=}$	Ni^{++}
$O^{=}$	Ni^{+++}	$O^{=}$	Ni^{++}	$O^{=}$
Ni^{++}	$O^{=}$	(X)	$O^{=}$	Ni^{++}
$O^{=}$	Ni^{++}	$O^{=}$	Ni^{++}	$O^{=}$

Figure 4. NiO defect structure in the case when the electron holes are associated with nickel ions on normal lattice positions, and conductivity occurs by exchange between bivalent or trivalent nickel ions.

$O^{=}$	Ni^{++}	$O^{=}$	Ni^{++}	$O^{=}$
Ni^{++}	$O^{=}$	Ni^{++}	$O^{=}$	Ni^{++}
$O^{=}$	Ni^{++}	$O^{=}$	Ni^{++}	$O^{=}$
Ni^{++}	$O^{=}$	($2e^{+}$)	$O^{=}$	Ni^{++}
$O^{=}$	Ni^{++}	$O^{=}$	Ni^{++}	$O^{=}$

Figure 5. NiO defect structure in the case when the electron holes are free and conductivity occurs by free movement of the electron holes inside the oxide.

where

$V_{Ni}^{=}$ = nickel vacancy

e^{-} = electron hole

NiO = ionic oxide with only bivalent nickel ions.

And the conductivity is thought to be due to a free movement of the electron holes in the oxide layer (Kofstad, D., 1966, p. 63).

Further increase in conductivity takes place with additions of lower valency cations and a decrease is observed with additions of higher valency cations. Kubaschewsky (1953, p. 31) reports that by adding 1 mole percent of Cr_2O_3 to NiO, the conductivity is decreased by three powers of ten, supposedly because the addition of Cr^{3+} ions to NiO lattice increases the number of cation defects, but decreases the number of trivalent Ni^{3+} ions (Figure 4) decreasing also the number of electron holes. As a consequence, the ionic conductivity increases, but the electron conductivity decreases. Also Smithelles, C., and others (1928, p. 269) found that the oxidation resistance in NiMo alloys decreased when reduced instead of electrolytic nickel was used due to the presence of sulfur (S^{+6}), and Kubaschewsky, O., (1953, p. 68) reported similar results when manganese (Mn^{7+}) and iron (Fe^{3}) were added in small quantities to electrolytic nickel. The kinetics of the NiO formation is given by the diffusion coefficients of oxygen and nickel in nickel oxide. Keefle, M., and Moore, J., (1961, p. 1438) report the

following values at constant pressure and temperatures below 1300°C:

$$D_o = 10^{-5} e^{-\frac{54,000}{RT}}$$

$$D_{Ni} = 1.83 \times 10^{-3} e^{-\frac{45,000}{RT}}$$

Kofstud, P., (1966, p. 125) reported the following equation for the diffusion coefficient of nickel in nickel oxide as a function of pressure:

$$D_{Ni} = B(P_{O_2})^{1/n}$$

where

B = diffusion coefficient at constant pressure, i.e. the values obtained from the above equations reported by Keefle and Moore

n = value higher than unity which depends on the pressure level.

As can be seen, this equation is similar to that given for the case of the electrical conductivity. The kinetics of the NiO formation leads to a parabolic behavior in oxidation, and its oxidation rate is given by the Wagner theory according to the following expression if the diffusion coefficient of oxygen is neglected as $D_o << D_{Ni}$ (Kofstad, P., 1966, p. 126).

$$K = AD_{Ni} \left[(P^o_{O_2})^{1/n} - (P^i_{O_2})^{1/n} \right]$$

where

K = oxidation rate

A = constant that depends on temperature

D_{Ni} = coefficient of diffusion of nickel in nickel oxide at constant pressure

$P^{o}_{O_2}$ = oxygen pressure at the oxide/oxygen boundary

$P^{i}_{O_2}$ = dissociation pressure of NiO

n = value depending on the pressure level and higher than unity

As nickel diffusivity is higher than oxygen diffusivity, the nickel concentration decreases from Ni/NiO boundary to NiO/O boundary more rapidly than does oxygen which decreases its concentration from NiO/O to Ni/NiO boundaries. If the oxygen pressure is constant, there will be a point along the layer thickness of the oxide where both nickel and oxygen concentrations justify the equilibrium constant for the equation of oxidation; wherever the dissociation pressure of NiO is equal to the oxygen pressure at the oxide/oxygen boundary, i.e., $P^{o}_{O_2} = P^{i}_{O_2}$, the oxide is being formed and grows inwardly (Fig. 6).

Calculations for dissociation pressure and initiation of oxidation in nickel are given in Appendix below the title "Thermodynamics in Nickel Oxide Formation." Finally, an example of parabolic oxidation in impure nickel is given in Figure 7 where the reaction rate is parabolic, as was predicted by the Wagner theory.

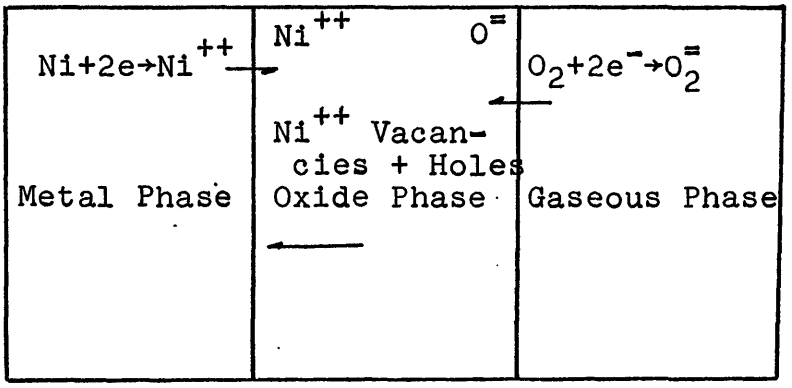

Figure 6. NiO as a p semiconductor. There is an excess of $O^{=}$ and a deficit of Ni^{++}. The conductivity increases with oxygen pressure and addition of lower valency cations.

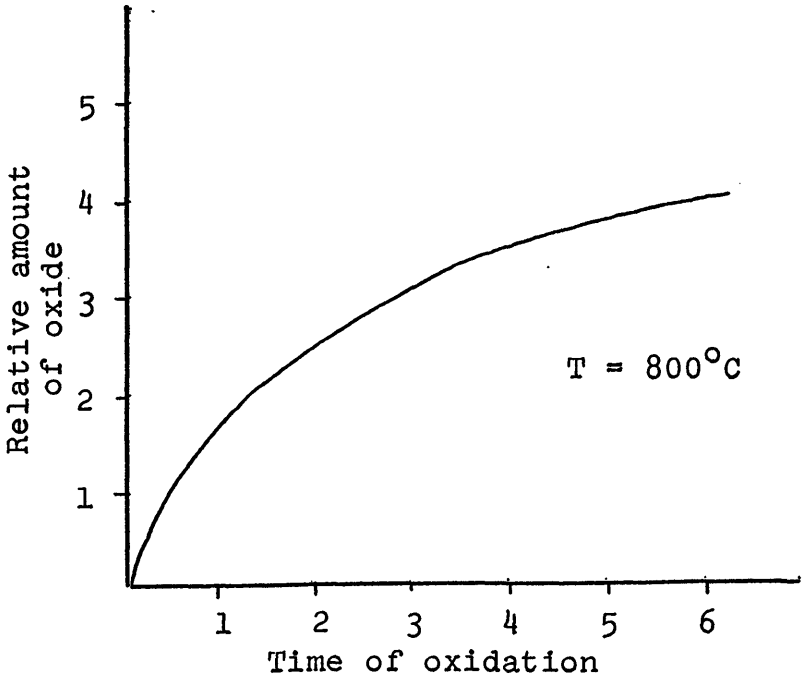

Figure 7. Parabolic oxidation of impure nickel.

Aluminum Oxide (Al_2O_3) - The aluminum oxide has been considered as a near-stoichiometric oxide at room temperature and normal pressure, an n semiconductor at high temperature and pressure less than 10^{-5} atmospheres of oxygen and a p semiconductor at high temperature and pressure greater than 10^{-5} atmospheres of oxygen. In the first case, the kinetics of oxidation depends on the ionic mobilities which are relatively low. The aluminum is therefore resistant to oxidation at these conditions. In the second case, the rate of oxidation depends on the number of electrons in the conduction band which are proportional to the number of aluminum interstitials (metal excess oxide). In the third case, the rate of oxidation depends on the number of electron holes in the conduction band which are proportional to the number of aluminum vacancies (Kofstad, P., 1966, p. 103).

Measurements of self-diffusion in Al_2O_3 were made by Paladino, A., (1962, p. 451) and Oishi, Y., (1957, p. 182) who reported the following equations.

$$D_{Al} = 28\, e^{-\frac{120.000}{RT}} \qquad 1670^{\circ}C - 1900^{\circ}C$$

$$D_O = 2 \times 10^{-3}\, e^{-\frac{152.000}{RT}} \qquad \leq 1600^{\circ}C$$

$$D_O = 6 \times 10^{-8}\, e^{-\frac{57.600}{RT}} \qquad > 1600^{\circ}C$$

The behavior of aluminum oxide as a p semiconductor is similar to the case of NiO which was explained above. The rate of oxidation will follow a parabolic curve and the

oxide will grow inwardly from the point where the exterior applied pressure is equal to the dissociation pressure of Al_2O_3. Now, considering Al_2O_3 a n semiconductor, the rate of oxidation decreases if the pressure of oxygen is increased, because the number of aluminum interstitials and at the same time the number of electrons in the conduction band is diminished (Fig. 8).

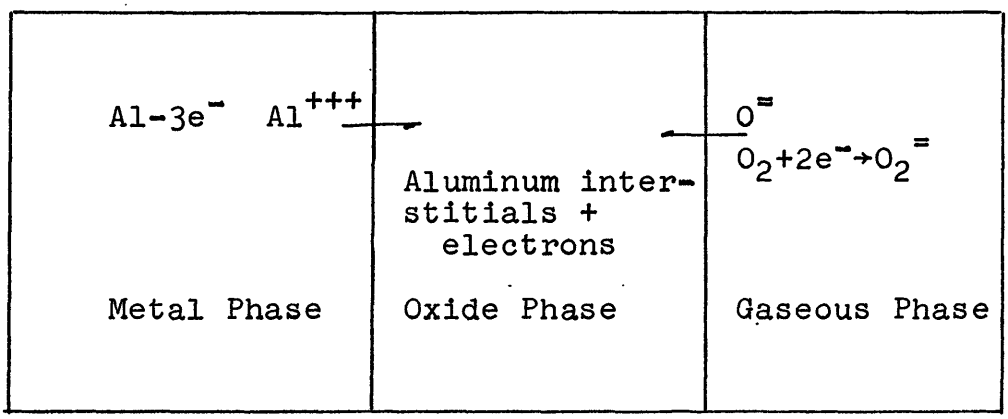

Figure 8. Al_2O_3 as n semiconductor; there is an excess of aluminum interstitials, and the electronic conductivity increases with additions of higher valence cations and decreases with additions of lower valency cations.

Molybdenum Oxides (MoO_2, MoO_3) - The molybdenum trioxide MoO_3 is an n semiconductor with molybdenum ions in excess. Additions of higher valency cations increase the electronic concentration, and additions of lower valency cations decrease it. If nickel or aluminum with 2 and 3 electrons in their valence bond go into MoO_3 which has

molybdenum ions with 6 electrons in its conduction band, the oxidation rate will be lowered because there is a tendency to the interstitial molybdenum to be destroyed and in this way the electronic conductivity will be diminished. The pressure of oxygen also tends to decrease the conductivity, but because metal molybdenum has low temperatures of vaporization and sublimation, the result is very different.

Kelley's equations for vaporization and sublimation are respectively: (Kelly, K., 1935, p. 71)

$$\log P \text{ (at)} = -11.820T^{-1} - 7.04 \log T + 30.494$$

$$\log P \text{ (at)} = -15.110T^{-1} + 1.46 \log T - 1.39 \times 10^{-3}T + 9.07$$

where

P = vapor pressure in atmospheres

T = temperature in kelvin degrees

And as is shown in Figure 9, the vapor pressure is equal to one atmosphere at 1151°C and because the oxidation experiments in this research are going to be at 1200°C, volatilization instead of diffusion will be the important factor to consider if a loss of weight is observed. In addition, MoO_3 tends to form eutectics with other oxides leading to catastrophic oxidation.

The MoO phase diagram shows that the stable oxide at high temperature is MoO_3 where MoO_2 is converted to MoO_3. Burns, R., and De Maria (1960, p. 1363) using a mass spectrometer method to study the sublimation of MoO_2 in the

MoO_3 vapor pressure (atm)	Temperature (°C)
0.0001	661
0.001	718
0.01	801
0.1	934
0.25	1000
0.50	1077
1.00	1151

Figure 9. MoO_3 vapor pressure calculated from Kelly's equation.

presence of Al_2O_3 at 1200°C, found that MoO_3 was formed and that no reaction between MoO_2 or MoO_3 and aluminum took place. Therefore, no aluminum-molybdenum oxide is to be expected in our case.

Binary Oxide Formation - Several spinnel-forming reactions have been studied using electromotive forces of galvanic cells:

(1) Nickel oxide reacts with aluminum oxide according to the following equation: $NiO + Al_2O_3 = NiAl_2O_4$. The thermodynamic and kinetic properties were calculated by Aleksandrovich, N., and Pavlovich, V., (1966, p. 93):

$$k = 3 \times 10^6 \, e^{-\frac{127.000}{RT}}$$

$$D_{Ni} = 3 \times 10^{-4} \, e^{-\frac{55.000}{RT}}$$

$$\Delta F(\text{Formation}) = -5.200 \text{ cal/mol} \quad (25^\circ C)$$

where:

k = reaction rate at high temperature

D_{Ni} = self-diffusion coefficient of nickel ions in $NiAl_2O_4$

ΔF = free energy of formation

(2) The nickel oxide reacts with molybdenum trioxide according to the following equation: $NiO + MoO_3 = NiMoO_4$. The same authors reported for this reaction an activation energy of 82.000 cal/mol which decreased to 54.000 cal/mol when chromium ions Cr^{+++} were added (1%), and because the Cr_2O_3 has the same structure and conductivity properties as Al_2O_3, the effect in our case might be similar if $NiMoO_4$ is formed in the oxide layer. On the other hand, if $NiMoO_4$ is not found it is because MoO_3 has been volatilized at high temperature before the spinnel reaction takes place.

No other compound oxide is to be expected according to thermodynamics of reactions between NiO, Al_2O_3, and MoO_3 or from the reported experiments given by Burns and De Maria, as cited before.

Phase Diagrams

As our alloys are going to contain molybdenum, nickel, and aluminum as basic components, it is useful to review the Ni-Al, Ni-Mo, Mo-Al, and Mo-Ni phase diagrams to predict the phases we will expect to find at several composi-

tions and heat treatments.

Nickel-Aluminum - The Ni-Al diagram has been determined except around the Ni_3Al phase where some authors disagree in their results.

Bradley, A.J. (1936, p. 51) and Hansen, N., (1958, p. 118) report an eutectic reaction taking place at 1385°C and 72 at % Ni, an ordered structure Ni_3Al existing from room temperature to 900°C and no peritectic reaction taking place at 1395°C.

Hansen, M. (1958, p. 118) reports the same eutectic reaction, but the ordered structure existing from room temperature up to 1395°C, and a perilectic reaction at 1395°C and 68 at % Ni (Figure 10).

Azou, P., (1966, p. 6) reports the eutectic and perilectic reactions at 1385°C and 1395°C respectively, with the ordered structured formed from room temperature up to 1390°C (Figure 11).

Elliot, R. P., (1965, p. 48) reports no ordering of Ni_3Al at high temperature when a third element is present.

Figure 12 shows the structure, reaction temperature, and compositions range for the phases in Ni-Al phase diagram.

Bradley, A., (1936, p. 63) found that the density of NiAl phase increases linearly from 45 to 56 % at Ni, but the lattice parameter increases from both extreme composition sides (2.862 A) to a maximum value (2.881) at 50% at Ni, concluding that:

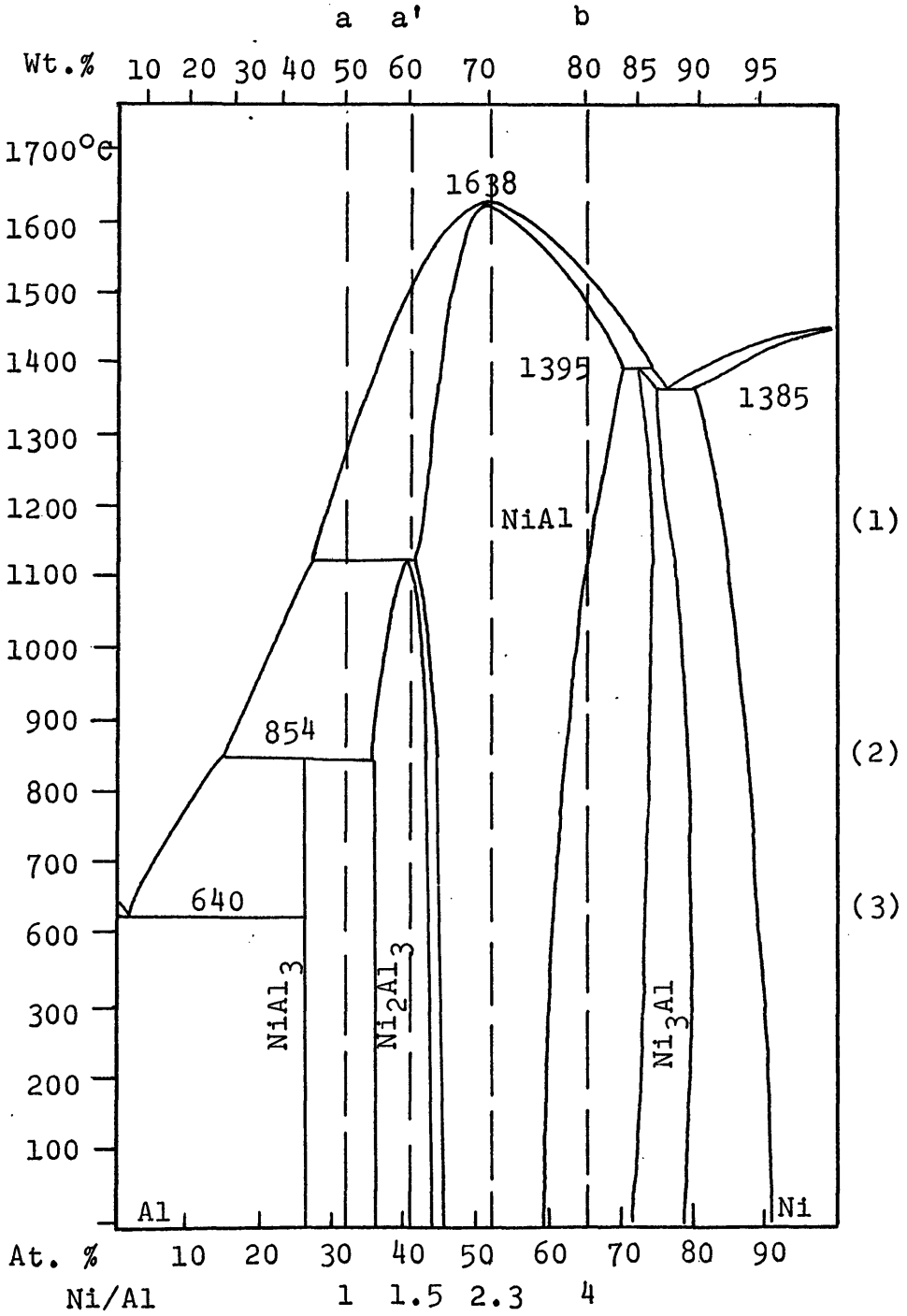

Figure 10. Al-Ni phase diagram. (From Constitution of Binary Alloys by Hansen.)

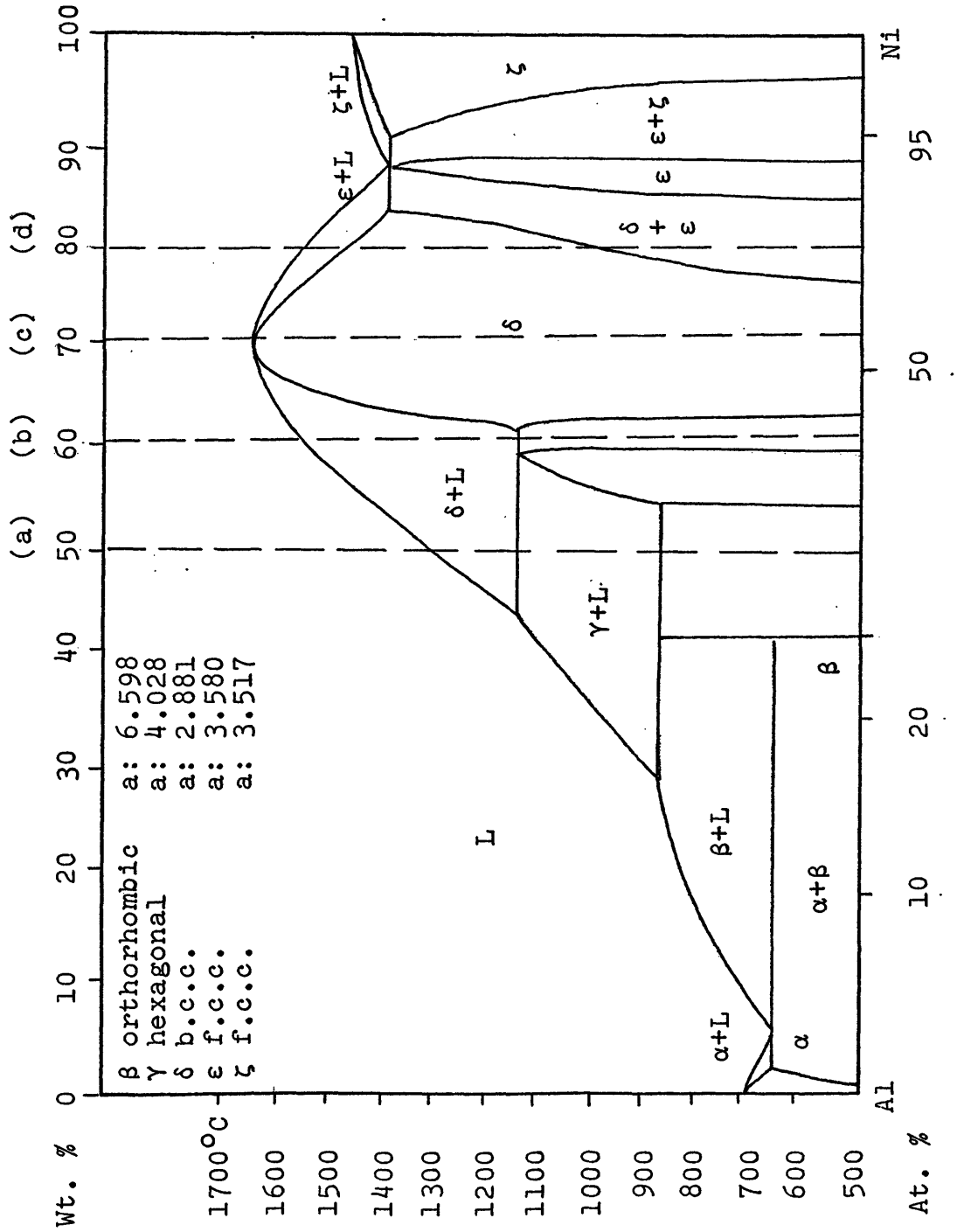

Figure 11. Al-Ni phase diagram. (From Diagrammes d'equilibre by Pierre Azou.)

Phase	Structure		Reaction Temp. °C	Composition	Source
$NiAl_3$	Orthorhombic	a: 6.598Å b: 7.352Å c: 4.807Å	854°C Peritectic	25 at.% Ni	Hansen, 1958, p. 115
$N_{12}Al_3$	Hexagonal	a: 4.028Å b: 4.891Å	1130°C Peritectic	35-45 at.% Ni at room T°	Hansen, "
NiAl	b.c.c.	a: 2.881Å	1630°C Congruent Point	45-56 at.% Ni at room T°	Hansen, "
Ni_3Al	f.c.c.	a: 3.580Å	1395°C Peritectic	72-80 at. % Ni at room T°	Hansen "

Figure 12. Characteristic of phases in Ni-Al system.

(1) The number of atoms per cell varies as the lattice parameter from 1.8 to 2.

(2) At 50% at. Ni, aluminum atoms are located at lattice corners and nickel atoms at lattice centers in an exact proportion 1:1 (CsCl structure).

(3) From 45 to 50% at. Ni, nickel vacancies in excess exist which are responsible for the number of atoms per cell lower than 2, and the decrease in lattice parameter.

(4) From 50 to 56 at. % Ni at replacement of large and light aluminum atoms by small and heavy nickel atoms are responsible for the decrease in lattice parameters and the increase in density, and the imperfect replacement of atoms will cause the number of atoms per cell to be less than 2.

Nickel-Molybdenum - The Ni-Mo diagram has been determined except at the dotted lines on Figure 13. The phases in this diagram are not well understood and frequently the results diverge as shown in Figure 14.

Aluminum-Molybdenum - As shown in Figure 15 neither the liquidus line around the congruent point nor the solidus line at the molybdenum side have been determined and, as before, there is also a discrepancy in data related with structures and parameters (Figure 16).

Aluminum-Nickel-Molybdenum - The Al-Ni-Mo ternary system has not been established.

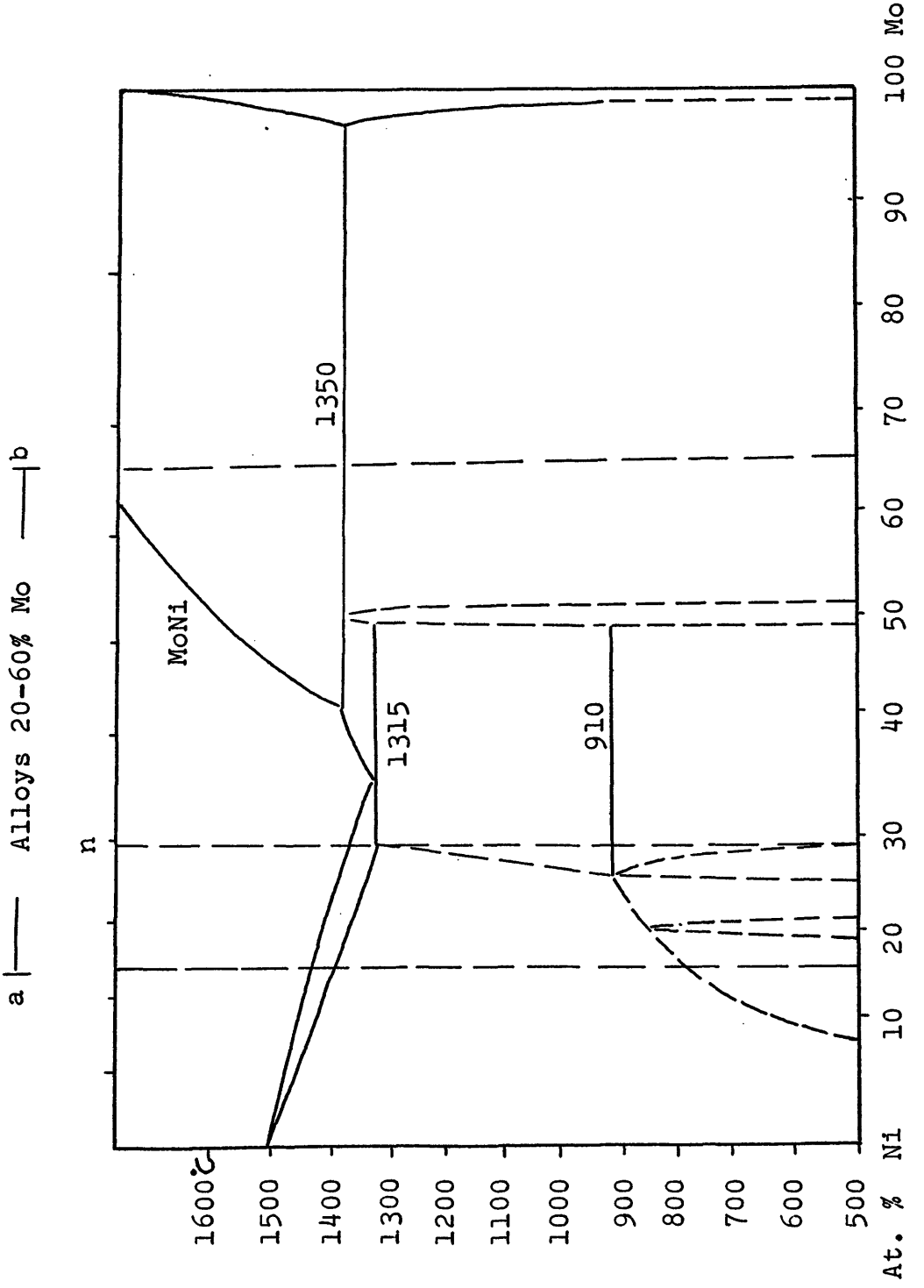

Figure 13. Ni-Mo phase diagram. (From Constitution of Binary Alloys by Hansen.)

Phase	Structure	Reaction Temp. °C	Composition	Source
$MoNi_4$	f.c.c. tetrogonal super lattice a: 3.62Å b: 3.57Å	860°C Peritectoid	20% at. Mo	Hansen, 1958, p. 968
$MoNi_4$	Tetragonal a: 5.683 b: 3.592	875°C Peritectoid	20% at. Mo	Shunk, F. 1969, p. 517
$MoNi_3$	Hexagonal a: 2.55 b: 4.20	910°C Peritectoid	25% at. Mo ± 1%	Hansen, 1958, p. 968
$MoNi_3$	Orthohexagonal a: 5.06 b: 4.22 c: 4.44	Not Given	Not Given	Taylor, A., 1962, p. 136
MoNi	Orthorhombic a: 9.108 b: 9.108 c: 8.85	1362°C Peritectic ± 2%	47% at. Ni	Shunk, 1969, p. 517
Ni_2	f.c.c.		Undetermined range	Shunk, 1969, p. 517

Figure 14. Characteristic of phases in Ni-Mo system.

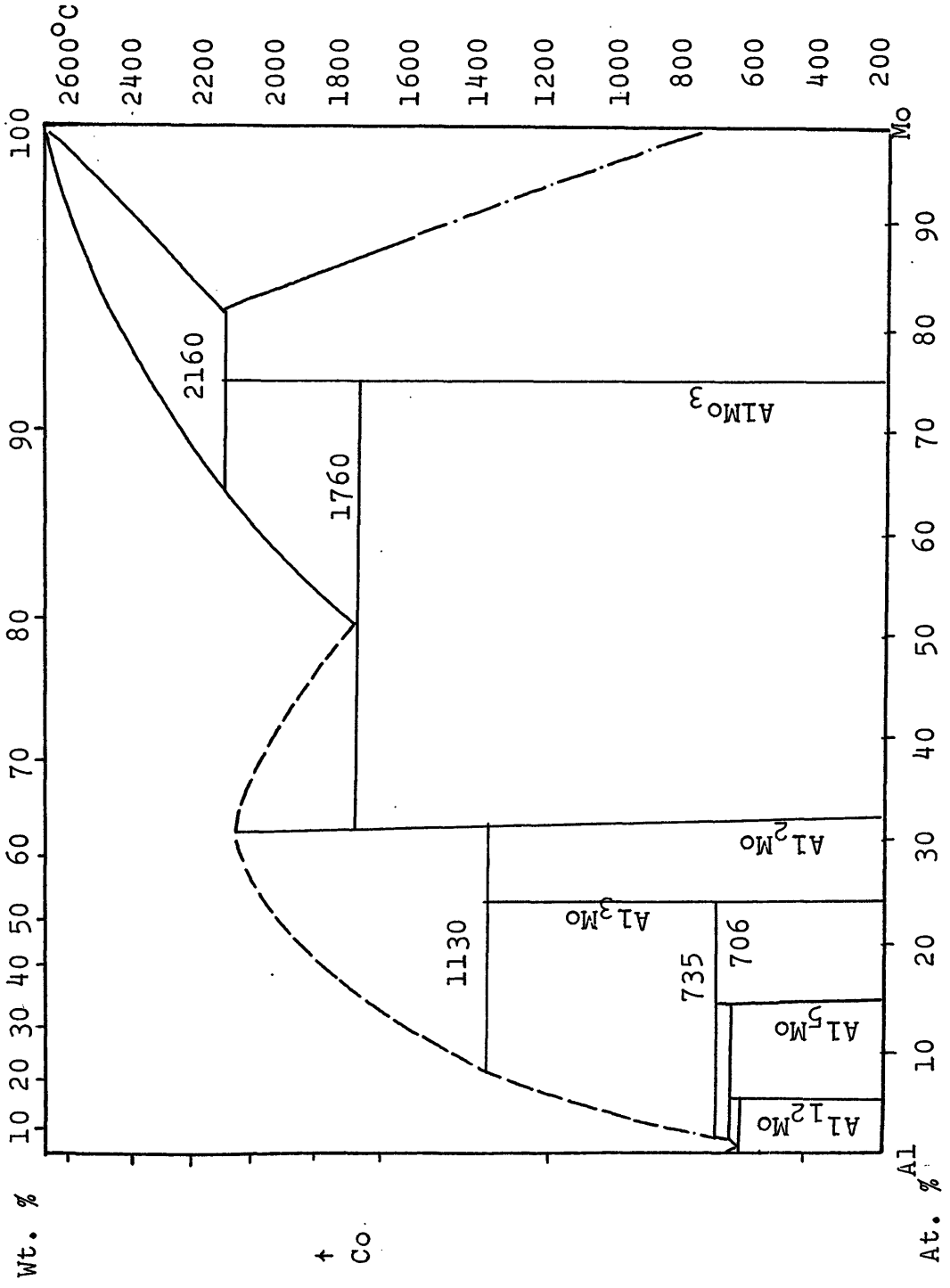

Figure 15. Al-Mo phase diagram. (From Constitution of Binary Alloys by Elliot.)

Phase	Structure		Reaction Temp. °C	Composition	Source
$Al_{12}Mo$	b.c.c. $Al_{12}W$ type	a: 7.57A	706°C Peritectic	0.78% wt. Mo	Elliot, R., 1965, p. 45
Al_7Mo	Monoclinic	a: 5.12 b: 13.0 c: 13.5 β: 95°	?	?	Elliot, R., 1965, p. 47
Al_6Mo		?	720°C Peritectic	?	
Al_5Mo	Hexagonal	a: 4.89 c: 8.8	900°C ?	?	Shank, 1969 p. 30
Al_4Mo	Monoclinic	a: 5.038 b: 17.737 c: 5.026 β: 100.83	1130°C Peritectic	20%	Elliot, 1965, p. 47
Al_2Mo	Unknown		2120	333% wt. Mo	Elliot, 1965, p. 45
Al_4Mo	C centered monoclinic	a: 5.255 b: 17.768 c: 5.225 β: 100.53	1130	20% wt. Mo	Shunk, 1969, p. 30
Al_3Mo	Tetragonal	a: 6.247 c: 10.000	1130 (P)	25% wt. Mo	Elliot, 1965, p. 47
Al_8Mo_3	C centered monoclinic	a: 9.164 b: 3.639 c: 10.04 β: 100.50	?	?	Shunk, 1965, p. 31

Figure 16. Characteristic of phases in Al-Mo system.

Phase	Structure		Reaction Temp. °C	Composition	Source
Al_8Mo_3	C centered monoclinic	a: 9.208 b: 3.63 c: 10.06 β: 100.47	?	?	Shunk, 1965, p. 31
$AlMo_3$	B-W structure	a: 4.95	2150°C (P)	75% wt. Mo	Hansen, 1958, p. 117

Figure 16. (Continued) Characteristic of phases in Al-Mo system.

EXPERIMENTAL PROCEDURE

The laboratory work was divided into two parts:

1) Study of alloys with molybdenum from 20% to 60%

2) Study of alloys with molybdenum up to 20%.

Alloys with molybdenum from 20% to 60% were first studied in order to acquire a general idea of the oxidation in Mo-Ni-Al alloys, and thereafter to study in more detail the more resistant to oxidation compositions.

Alloys with Molybdenum from 20% to 60%

The following general sequence was performed in this part of the laboratory work:

a) melting

b) remelting

c) heat treatments

d) oxidation tests

a) Sixteen alloys were made with the following compositions: 1.0, 1.5, 2.3, 4.0, Ni/Al weigh ratio plus 20%, 30%, 40%, and 60% of molybdenum in weight. These alloys are shown as open circles in Figure 17 and their relative percentages are tabulated in Table 1 of the appendix from alloy 33 to alloy 48. Also, Figure 11 indicates the nickel-aluminum ratios as a, b, c, and d, discontinuous lines.

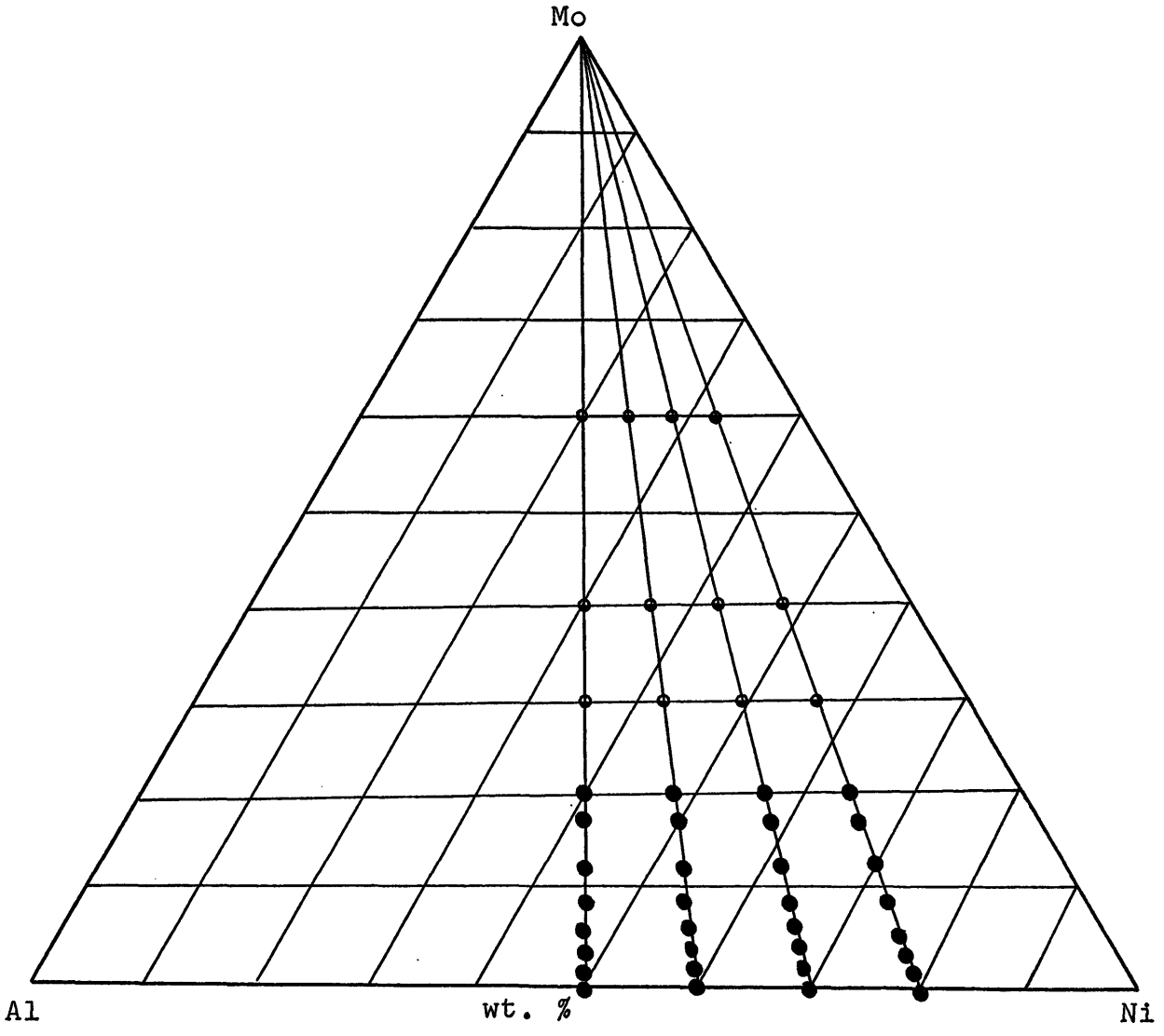

Figure 17. Al-Mo-Ni composition triangle. The circles are for alloys 20%-60% in molybdenum. The dots are for alloys up to 20% in molybdenum.

The starting materials were:

Al: Commercial pure aluminum (2s)

Ni: Commercial pure nickel (grade A)

Mo: 99.99% purity

and the reported impurities were:

Al: 1.0% Si maximum

0.2% Cu maximum

0.1% Mn maximum

Ni: 0.25% Cu maximum

0.4% Fe maximum

0.35 Mn maximum

0.01% S maximum

0.15% C maximum

Weighed proportions of these elements were melted in a levitation furnace. An inert atmosphere (argon) inside the melting furnace was used to keep impurities to a minimum. For each alloy the melting furnace was evacuated twice up to 20 in. Hg vac. and filled with argon up to 6 psig. These figures were limited by a hazard in blowouts.

b) Subsequently the samples were remelted twice at the same conditions as before to assure complete homogeneity in composition throughout the sample. This must be done although the magnetic force produces a stirring effect on the sample, and the time for melting and stirring is very short. It was approximately 10 sec for melting and 50 sec for stirring; otherwise the furnace becomes overheated.

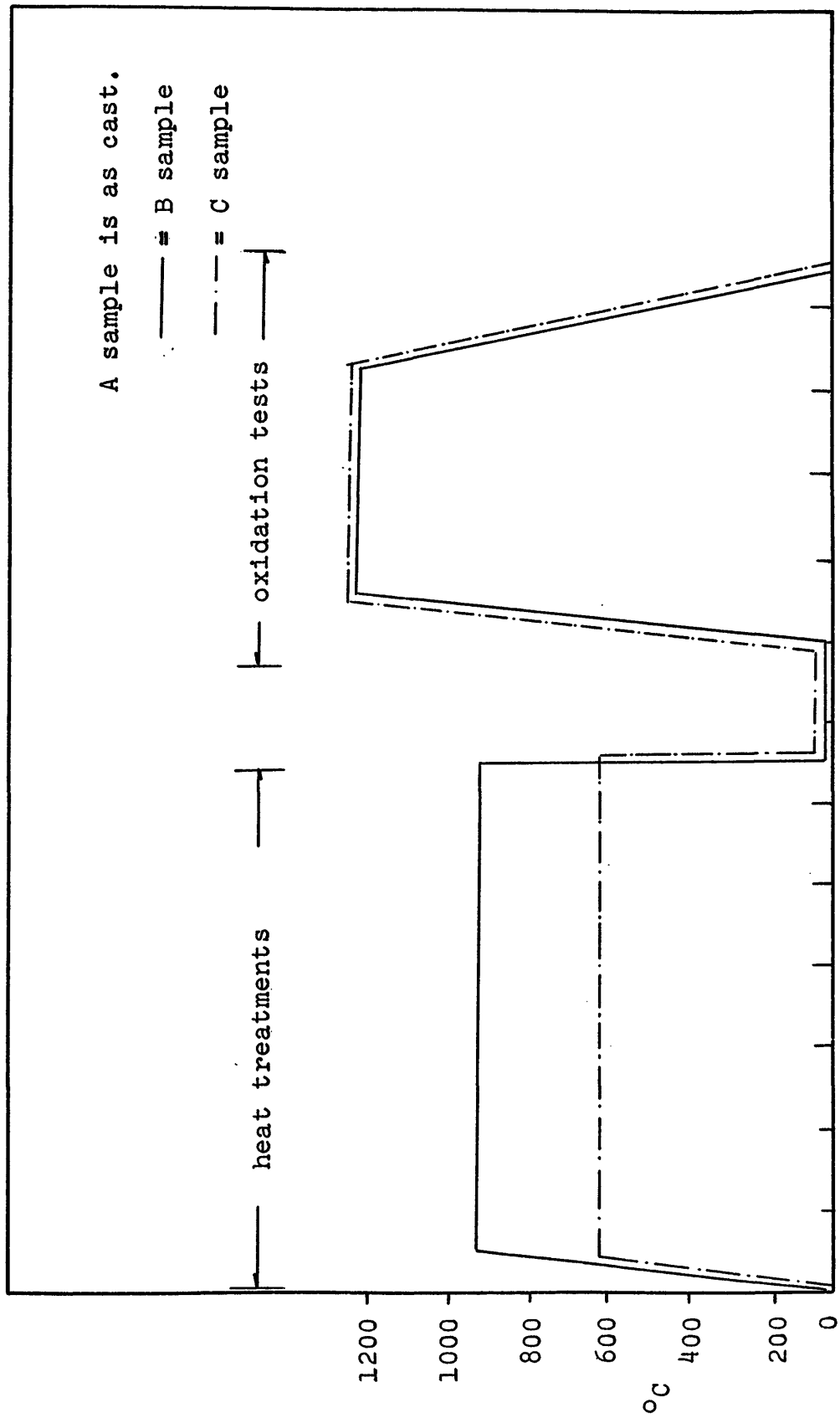

Figure 18. Heat treatments and oxidation tests for alloys 20% to 60% in molybdenum.

After remelting, samples solidified in a copper mold placed below the coil. The average sample was 6 mm in diameter, 6 mm high and weighed 1.4 grams.

c) Heat treatment cycles were performed on each composition in order to study the effect of the microstructure on oxidation at high temperature. Figure 18 graphs temperature versus time for the following samples.

1. Heat treatment on A samples: as cast
2. Heat treatment on B samples: annealing at 900°C during 60 hours and quenching in cold water
3. Heat treatment on C samples: annealing at 600°C during 60 hours and quenching in cold water.

As the samples were brittle, they could not be strain annealed in order to achieve rapid recrystallization and the soaking time inside the furnace had to be long (60 hours). Argon gas was leaked into the furnace in an attempt to reduce oxidation during this stage.

d) The oxidation test was performed at 1200°C using the same furnace but at oxidizing conditions. The oxidation time lasted for 30 hours, at the end of which a furnace cooling followed to avoid thermal stress scaling.

Alloys With Molybdenum up to 20%

The following general sequence was performed in this part of the laboratory work:

a) melting

b) remelting

c) checking for losses in weight

d) checking for copper contamination

e) heat treatments

f) mounting, grinding, and etching

g) oxidation test

h) x-ray analysis

a) Thirty-two alloys were prepared with the following compositions: 1.0, 1.5, 2.3, 4.0 Al/Ni plus 1.5, 3.0, 5.0, 8.0, 13.0, 17.0, and 20% wt. of molybdenum. These compositions are shown as dots on Figure 17 and their relative percentages are tabulated on Table 1 in the appendix (alloys 1 to 32). They were chosen according to the results obtained in the first part where 20% in molybdenum produced the less oxidized alloys, as will be explained later.

The starting materials in this case were:

Al: 99.99 purity

Mo: 99.99 "

Ni: 99.99 "

b) Identical melting and remelting techniques as for alloys 20-60% were used. The average weight obtained was 1.6 grams.

c) Possible changes in composition were checked by weighing the samples after remelting and a 0.5% maximum difference in weight was observed in alloys with 2.3 and 1.5 Ni/Al. This

loss is considered normal due to the high energy of formation of the NiAl phase which causes sublimation in the alloy.

d) Possible copper contamination coming from the copper mold used in solidification was checked with a Perkin-Elmer atomic absorption spectrometer, and no contamination was found.

e) Heat treatments on each composition were made to study the effect of microstructure in oxidation. Figure 19 explains the way they were performed in order to obtain A, B, C, and D samples:

1. Heat treatment in A samples: as cast
2. Heat treatment in B samples: annealing at 1200°C during 60 hours and water quenching. Argon gas was leaked into the furnace for the same purpose as for alloys 20-60% Mo.
3. Heat treatment in C samples: annealing at 900°C for 60 hours and water quenching.
4. Heat treatment in D samples: annealing at 900°C for 60 hours and furnace cooling at 60°/hr.

f) As the samples were small in size, it was necessary to get a bakelite support for grinding, polishing, etching, and observing in the microscope. Figure 20 explains the way the samples were mounted.

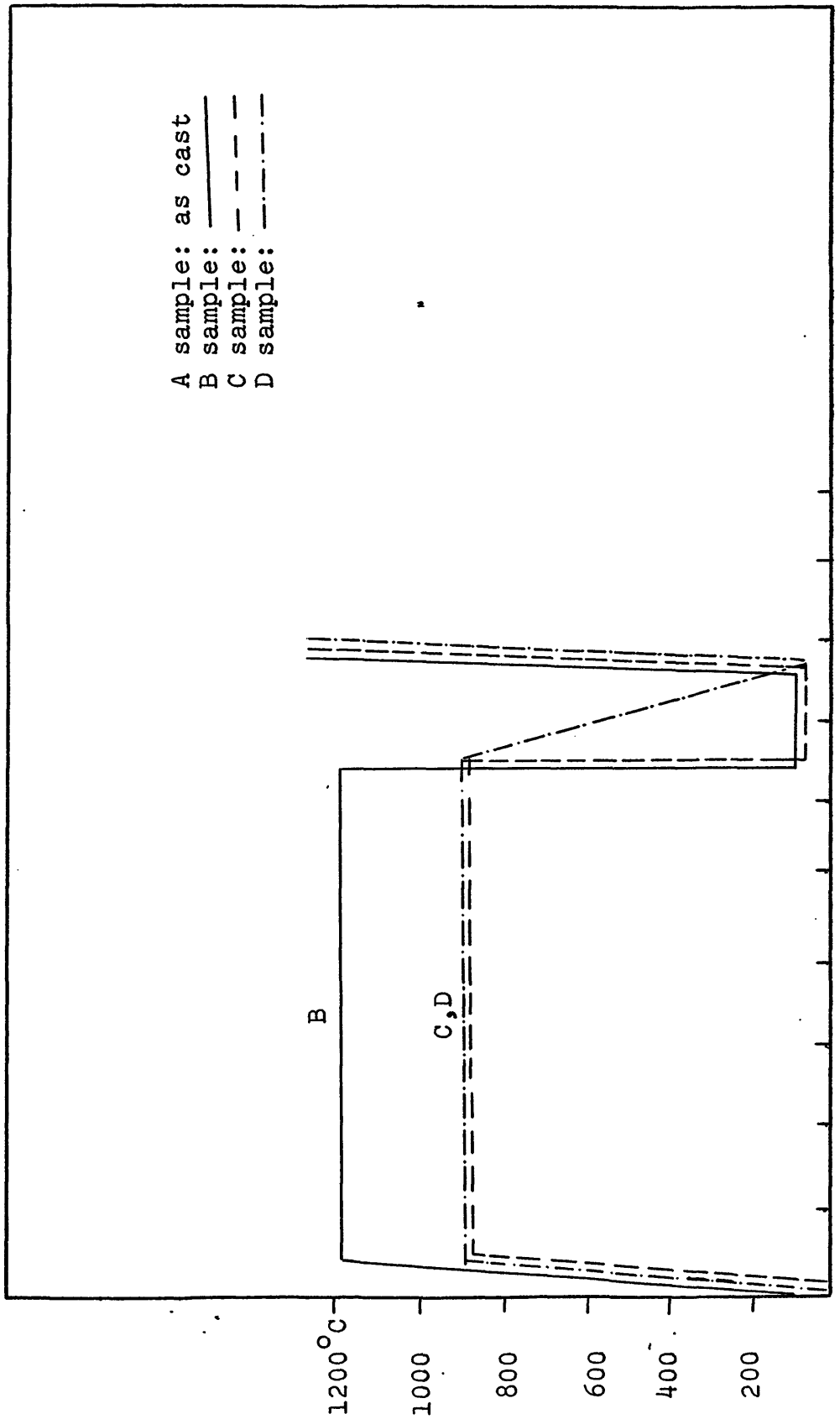

Figure 19. Heat treatments for alloys with Mo up to 20%.

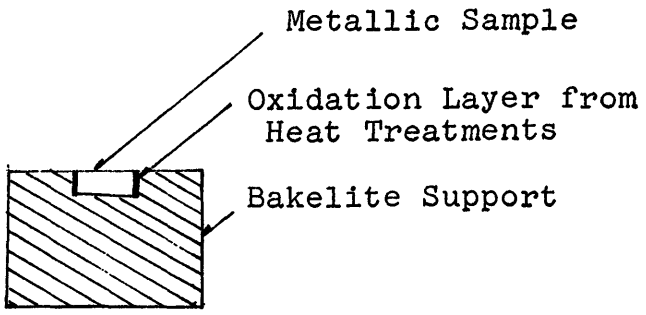

Figure 20. Mounting of samples in bakelite. Scale 1:1.

Polishing was done with powdered magnesium oxide, and the samples were etched in a solution 30% nitric acid in water at 70°C for 20 seconds.

g) Some characteristic alloys were drawn out from the bakelite support and placed on a hot stage furnace. The samples had to be ground in order to fit the 8 mm diameter by 3 mm high micro furnace stage. The conditions for the oxidation test were:

1. An initial constant flow of argon was maintained over the sample during heating up to 1200°C to prevent oxidation at temperatures lower than 1200°C.

2. Once this temperature was attained, oxygen was allowed into the furnace at a pressure of 1 atmosphere and simultaneously the argon flow was cut off.

3. A photographic record was taken at different periods of oxidation or whenever a phase change occurred. This was accomplished by use of an orthomat camera attached

to the microscope. A silica disk closed the hot stage, protecting the lens from heating and isolating the sample from the surrounding atmosphere (Figure 21).

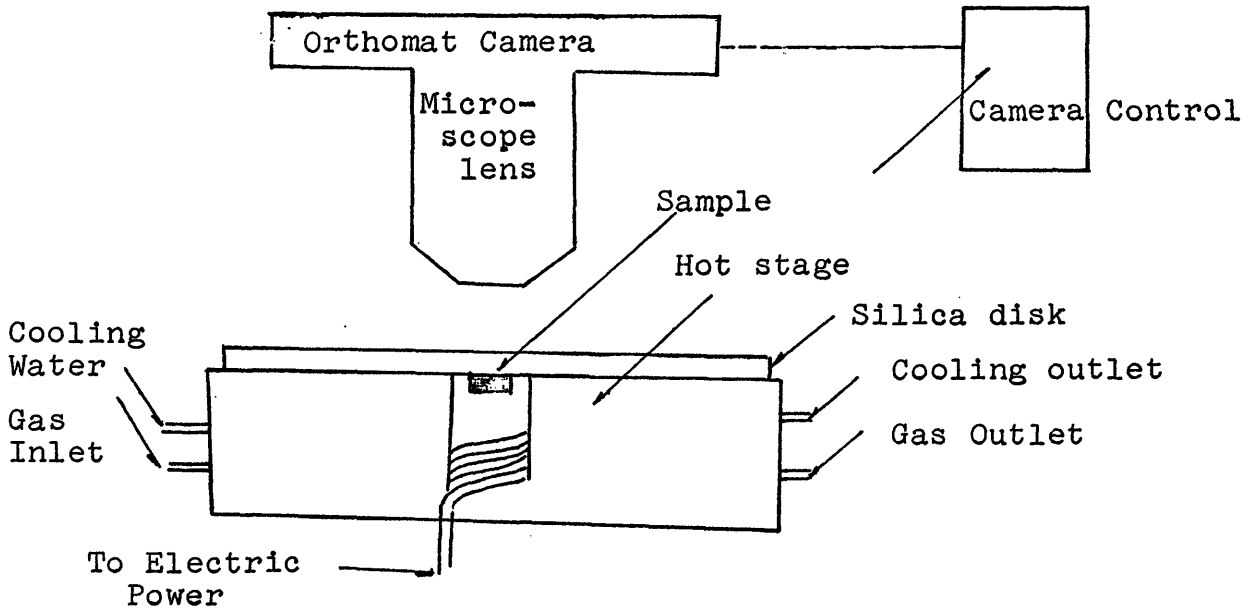

Figure 21. Hot stage and orthomat camera set-up.

h) X-ray diffraction tests were made on some samples according to the results obtained in parts e) and g) of this section. A Debye Schereer camera with filtered copper radiation was used and the samples for these x-ray tests were obtained by grinding to -300 mesh, gluing with plastic cement (no x-ray interference), rolling up to get a 0.3 mm diameter by 1 cm long thin rod, and finally drying at room temperature. X-ray patterns of nickel, oxide, aluminum oxide, molybdenum oxide and binary alloys

with 1.0, 1.5, 2.3, 4.0 nickel-aluminum weight ratio were obtained to facilitate the lines identification by the superposition method.

EXPERIMENTAL RESULTS

Alloys 20% to 60% in Molybdenum

Samples A - As is shown in Figure 22, no composition was resistant to oxidation at 1200°C, although a slight difference in oxide color was observed in alloys with 20% molybdenum; it was green-blue instead of blue-yellowish. The oxides were, in general, very soft and not adherent.

Samples B - Figure 23 shows the oxide characteristics for these samples after heat treatment at 900°C. As in the A samples there is also a difference in color with molybdenum content. Posterior oxidation test at 1200°C produced a change in color of the oxide, especially in alloys with 20% molybdenum, in such a way that no difference in oxidation could be observed in samples A or B after oxidation tests at 1200°C for compositions higher than 20% in molybdenum, but a more oxidized layer was formed in B samples after oxidation tests and with compositions 20% in molybdenum. The yellowish color seems to be a characteristic of the most oxidized layers coincident with high molybdenum content.

Samples C - Better oxidation resistance during heat treatment at 600°C was observed in these samples. The resultant oxide was black, hard, compact and uncracked for alloys 20% in molybdenum, and green-blue, soft and not adhered to the substratum for alloys higher than 20% in

molybdenum (Figure 25). Oxidation tests at 1200°C again produced the characteristic yellowish color already observed in A and B samples when oxidized at the same conditions (Figure 26).

It is important to state that no melting was observed in A, B, or C samples during heat treatment or oxidation tests, as would be expected for alloys with 1.0 and 1.5 Ni/Al weight ratio. In fact, there was no change in shape, nor hole formation by supposed evaporation.

Given the limitations in data acquired by visual observation of color, hardness and adherence of the oxide layer, little can be established about the role of the microstructure obtained (if any) in heat treatments or the effect of aluminum content on the oxidation behavior at high temperature. Nevertheless, it was observed that the effect of molybdenum and a low concentration of it (20%) was found to be the best. For this reason, it was thought that a more detailed study of alloys with molybdenum less than 20% was necessary in order to find out the effect of composition and previous heat treatment on the oxidation behavior. The laboratory sequence for these alloys was explained above and the results are given in the next section.

Ni/Al	20	30	40	60 % Mo wt.
1.0	green-blue soft non-adhered	blue-yellowish very soft non-adhered	blue-yellowish very soft non-adhered	blue-yellowish very soft non-adhered
1.5	green-blue soft non-adhered	blue-yellowish very soft non-adhered	blue-yellowish very soft non-adhered	blue-yellowish very soft non-adhered
2.3	green-blue soft non-adhered	blue-yellowish very soft non-adhered	blue-yellowish very soft non-adhered	blue-yellowish very soft non-adhered
4.0	green-blue soft non-adhered	blue-yellowish very soft non-adhered	blue-yellowish very soft non-adhered	blue-yellowish very soft non-adhered

Figure 22. Color, hardness, and adherence of the oxides in as-cast samples (A samples) when oxidized at 1200°C during 30 hours.

Ni/Al	20	30	40	60 % Mo
1.0	green-blue soft non adhered	blue-yellowish very soft non adhered	blue-yellowish very soft non adhered	blue-yellowish very soft non adhered
1.5	green-blue soft non adhered	blue-yellowish very soft non adhered	blue-yellowish very soft non adhered	blue-yellowish very soft non adhered
2.3	green-blue soft non adhered	blue-yellowish very soft non adhered	blue-yellowish very soft non adhered	blue-yellowish very soft non adhered
4.0	green-blue soft non adhered	blue-yellowish very soft non adhered	blue-yellowish very soft non adhered	blue-yellowish very soft non adhered

Figure 23. Color, hardness, and adherence of the oxides formed during heat treatment at 900°C in alloys with Mo from 20% to 60% as a function of the composition (B samples).

Ni/Al	20	30	40	60% Mo
1.0	blue-yellowish very soft non adhered	blue-yellowish very soft non adhered	blue-yellowish very soft non adhered	blue-yellowish very soft non adhered
1.5	blue-yellowish very soft non adhered	blue-yellowish very soft non adhered	blue-yellowish very soft non adhered	blue-yellowish very soft non adhered
2.3	blue-yellowish very soft non adhered	blue-yellowish very soft non adhered	blue-yellowish very soft non adhered	blue-yellowish very soft non adhered
4.0	blue-yellowish very soft non adhered	blue-yellowish very soft non adhered	blue-yellowish very soft non adhered	blue-yellowish very soft non adhered

Figure 24. Color, hardness, and adherence of the oxides of B heat treated samples when oxidized at 1200°C during 30 hours.

Ni/Al \ % Mo	20	30	40	60 % Mo
1.0	black hard adhered	green-blue soft non adhered	green-blue soft non adhered	green-blue soft non adhered
1.5	black hard adhered	green-blue soft non adhered	green-blue soft non adhered	green-blue soft non adhered
2.3	black hard adhered	green-blue soft non adhered	green-blue soft non adhered	green-blue soft non adhered
4.0	black hard adhered	green-blue soft non adhered	green-blue soft non adhered	green-blue soft non adhered

Figure 25. Color, hardness, and adherence of the oxides formed during heat treatment at 600°C in alloys with Mo from 20% to 60% as a function of the composition (C samples).

Ni/Al	20	30	40	60 % Mo
1.0	green-blue soft non adhered	blue-yellowish very soft non adhered	blue-yellowish very soft non adhered	blue-yellowish very soft non adhered
1.5	green-blue soft non adhered	blue-yellowish very soft non adhered	blue-yellowish very soft non adhered	blue-yellowish very soft non adhered
2.3	green-blue soft non adhered	blue-yellowish very soft non adhered	blue-yellowish very soft non adhered	blue-yellowish very soft non adhered
4.0	green-blue soft non adhered	blue-yellowish very soft non adhered	blue-yellowish very soft non adhered	blue-yellowish very soft non adhered

Figure 26. Color, hardness, and adherence of the oxides of C heat treated samples when oxidized at 1200°C during 30 hours.

Alloys Up to 20% Molybdenum

The experimental results for these alloys are given in three sections:

A. Results obtained in heat treatments

B. Results obtained in oxidation tests

C. Results obtained in x-ray analysis

A. Results Obtained in Heat Treatments

As a neutral atmosphere could not be achieved in heat treatments, some oxidation occurred and the oxide layers will be compared to those already seen on A, B, and C samples with 20-60% in molybdenum.

B Samples - The heat treatment performed on these samples is explained in Figure 19 and the resultant oxide layers are shown in Figure 27. As can be seen, they are black, hard, and adherent for those compositions between A-B and C-D discontinuous lines. This composition field then encloses the most oxidation resistant alloys for these particular conditions. At the left of the line A-B melting was observed and at the right of the line C-D the oxide was green or brown, hard but sometimes scaled and even soft, therefore not protective. If these results are compared with those given in Figure 22 when as-cast alloys were oxidized at the same temperature level and for 30 hours (Fig. 18), it can be concluded that there is a region in composition around 20% in molybdenum where the as-cast

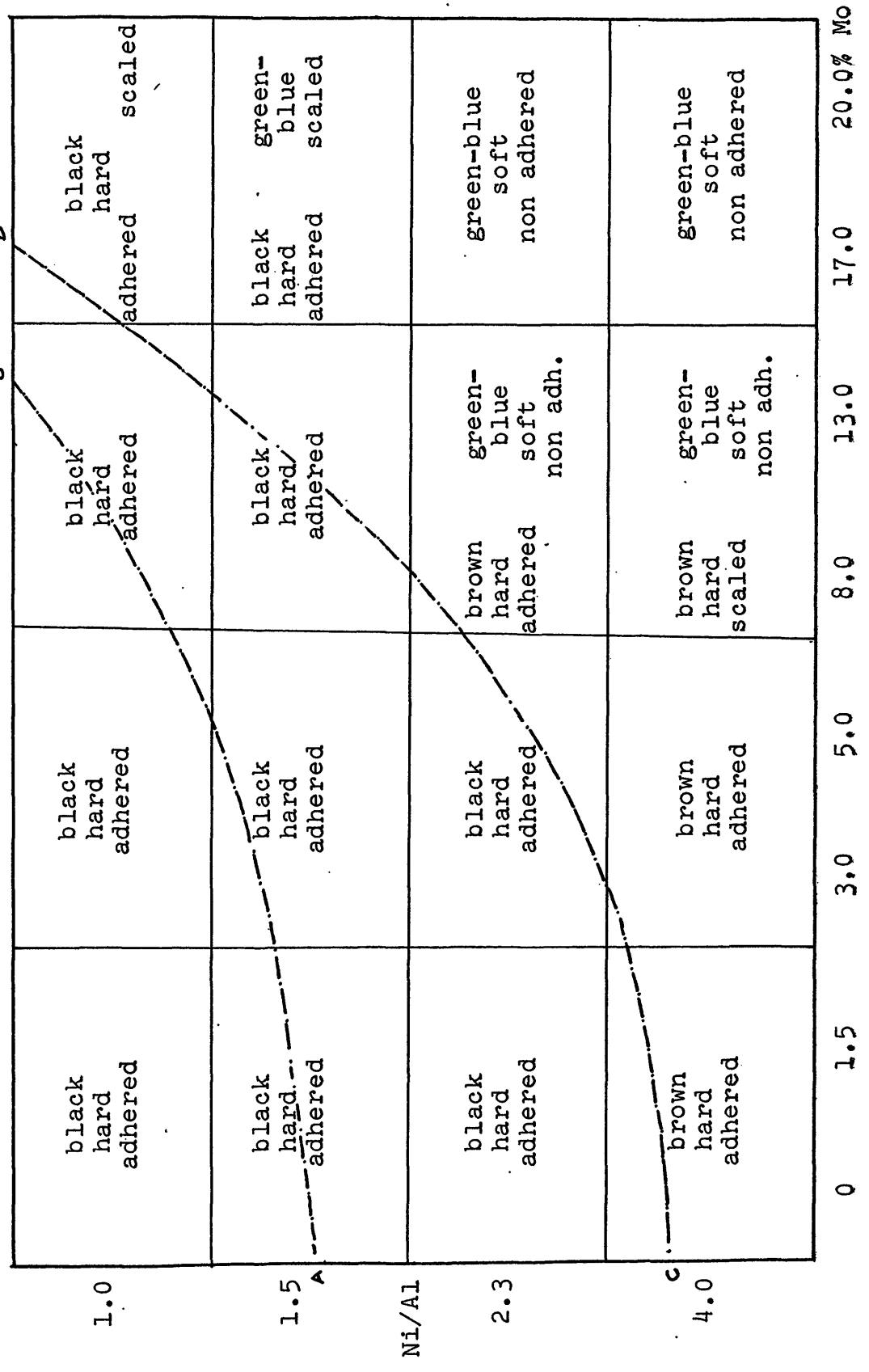

Figure 27. Color, hardness, and adherence of oxides formed in heat treatment at 1200°C (B samples).

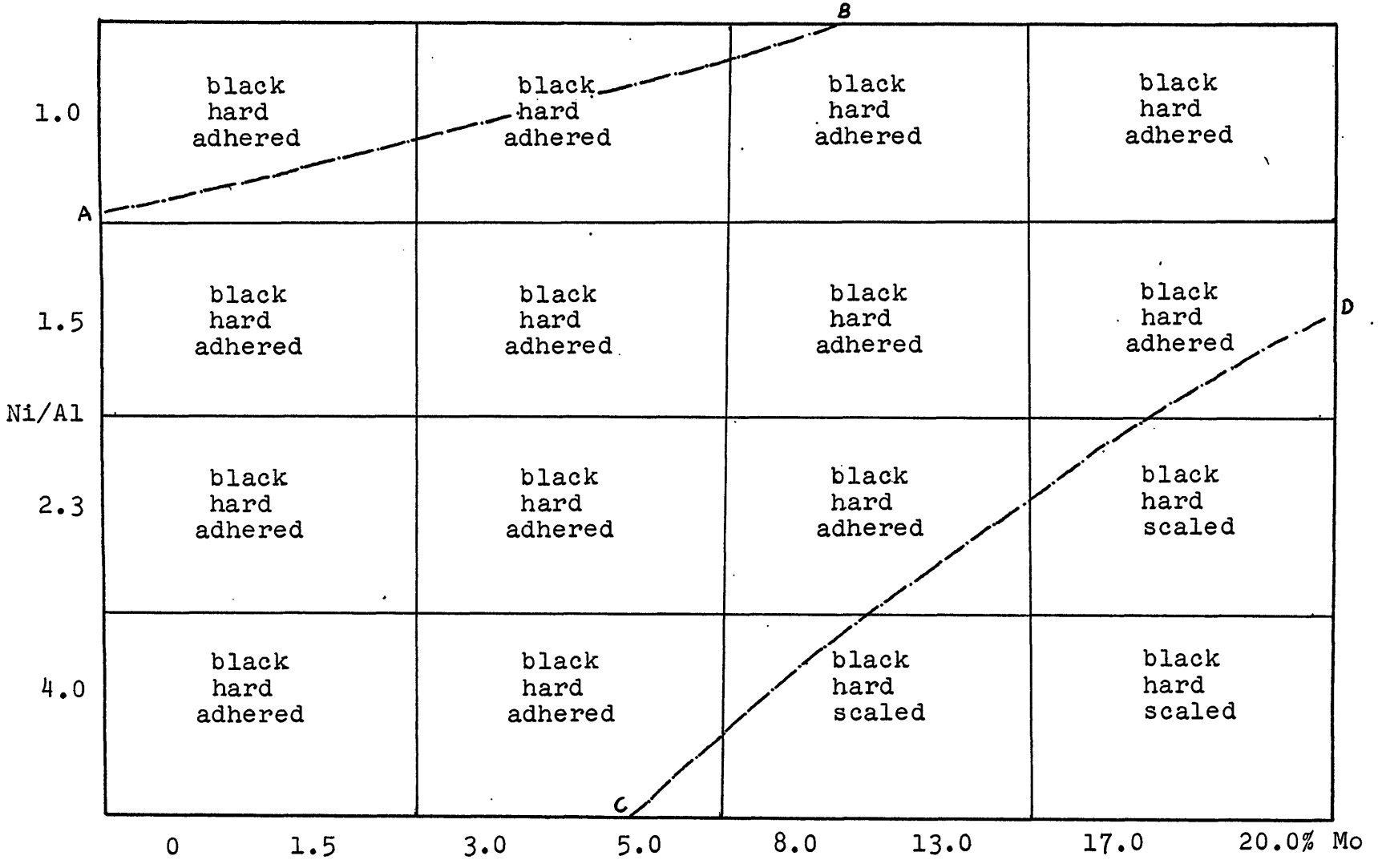

Figure 28. Color, hardness, and adherence of oxides formed in heat treatment at 900°C (C and D samples).

microstructure show better resistance to oxidation at 1200°C and also that this resistance depends on the nickel-aluminum ratio.

C Samples - The heat treatment performed on these samples is explained in Figure 19 and the resultant oxide layers are shown in Figure 28. A broader composition field was found in this case because of the lower temperature in heat treatment. As in B samples A-B and C-D also encloses the useful composition field at high temperature, while at the left of AB, melting was observed and at the right of CD, a less protective oxide layer was formed. If these results are compared with those given in Figure 23 where heat treatments at the same conditions were performed on alloys 20-60% in molybdenum, the following results are obtained.

a. Alloys higher than 20% in molybdenum were less resistant to oxidation during heat treatments.
b. The melting point of the alloys increased with molybdenum content.
c. The black oxides seem to be the most protective except in cases of melting and scaling.
d. Powdered yellowish oxide was formed at high molybdenum content where oxidation was most severe.

D Samples - The heat treating performed on these samples was similar to C samples except for the cooling after heating which was furnace cooling. The resultant oxide layers are also given in Figure 28 as no difference

was seen between C and D samples.

B. Results Obtained in Oxidation Tests

The results obtained in oxidation tests are given in the following order:

1. Results obtained in alloys with 4.0 Ni/Al weight
2. Results obtained in alloys with 2.3 Ni/Al weight
3. Results obtained in alloys with 1.5 Ni/Al weight
4. Results obtained in alloys with 1.0 Ni/Al weight

1. Results obtained in alloys with 4.0 Ni/Al weight: Figures 29-31 show oxidation behavior in as cast alloys and molybdenum 0, 1.5, and 3.0% weight when they were tested in oxidation at one atmosphere oxygen pressure, 1200°C and for one minute. As it is seen, oxidation increases with time and molybdenum content, and a volatile oxide seems to be formed. Figures 32-35 show the oxidation behavior in as cast alloys with 8% molybdenum when tested in oxidation at one atmosphere oxygen pressure, 1200°C and for 0, 1, 1.5, 2.0 minutes: the oxidation increases with time and a volatile oxide seems to be formed. Conclusion: Alloys with 4.0 Ni/Al weight are not resistant to oxidation at 1200°C, and the more molybdenum that is added, the greater is the oxidation rate. The volatile oxide is a compound of molybdenum, probably MoO_3, as was explained in the literature survey.

2. Results obtained in alloys with 2.3 Ni/Al weight: Figures 36-38 show oxidation behavior in heat treated samples at 1200°C (B samples) without addition of molybdenum when tested in oxidation at one atmosphere oxygen pressure, 1200°C, and for 0, 1/2, 1 minute: the alloy is resistant to oxidation at these conditions. Figures 39-41 show oxidation in as cast alloys with 3% molybdenum when tested in oxidation at one atmosphere oxygen pressure, 1200°C and for 0, 1, 2 minutes. This alloy is less resistant than the former without molybdenum and again the volatile oxide seems to be formed. Figures 42-45 show oxidation in B heat treated samples with 20% in molybdenum, when tested in oxidation at one atmosphere oxygen pressure, 1200°C and 0, 1/2, 1, 2.0 minutes; still more oxidation is formed and it is heterogeneous. Conclusion: Alloys with 2.3 Ni/Al weight are oxidation resistant when no molybdenum is present. Additions of molybdenum produce a highly volatile oxide.

3. Results obtained in alloys with 1.5 Ni/Al weight: Oxidation tests were performed on an as cast alloy with 3% in molybdenum. Figures 46-48 show the melting at interdendritic spots; the sample was not heated up to 1200°C but up to the temperature where melting began and could be observed. Conclusion: Alloys with 1.5 Ni/Al weight and low percent in molybdenum (3% Mo) are useless at high

temperatures where low melting point rather than oxidation is the limiting factor.

4. Results obtained in alloys with 1.0 Ni/Al weight: Figures 49-51 show the melting in zones surrounding the first solid formed in solidification (probably NiA) in a sample 1.0 Ni/Al weight without molybdenum. X-ray analysis showed there to be NiAl, $NiAl_3$, and Ni_2Al_3 in this alloy, but as the previous heat treatment was performed at 1200°C, it is thought that the cooling rate was not sufficiently rapid to freeze most of the original structure (NiAl). This is due to the small volume of the sample, so that phase transformations occur while it is transported from the furnace to the cooling medium. If this occurred the first solid to melt in oxidation test will be $NiAl_3$ and the second will be Ni_2Al_3.

When 3% molybdenum is added as third component, the results in as cast and B heat treated samples when tested in oxidation is shown in Figures 52-58. Again, B samples melted before 1200°C and, consequently, their utility is limited to low temperatures. The B sample is quite similar to those already observed in alloys without molybdenum (same Ni/Al w.r) and the A sample (as cast) shows a fine dendritic formation. Finally, Figures 59-62 show the effect of adding 13% molybdenum in A and B samples. The peritectic reaction here disappeared and, consequently, melting

was not observed up to 1200°C. Oxidation test for two minutes did not result in apparent change in the surface of as cast or B samples; consequently, this composition is considered the most resistant in oxidation at high temperature. The white zone seen in Figures 61 and 62 was caused by a dimming of the silica disk (hot stage window) in previous oxidation tests. Conclusion: the compositions with better resistance to oxidation at high temperature are located around 13%-17% molybdenum and 1.0-1.5 Ni/Al. The finer the coring and the higher the observed melting point, the higher the molybdenum content, indicating that there exists a possible shift of the NiAl phase diagram toward the aluminum side with additions of molybdenum.

The oxidation tests were performed on the middle of polished and etched samples in order to avoid the interference of the previous oxidation in heat treatments. This previous oxidation shows the real role of the microstructure at long periods of time as 60 hours, as is seen in Figures 63-65. In Figure 63, it can be seen that preferred oxidation proceeded along grain boundaries in a 4.0 Ni/Al with 3% molybdenum alloy during heat treatment at 1200°C; in Figure 64 it can be seen that homogeneous oxidation was the dominant in a 2.3 Ni/Al with 1.5% molybdenum alloy; and, finally, Figure 65 shows that preferential oxidation along a crack left white zones by effect of an impoverishment of one element.

C. Results Obtained in X-Ray Analysis

The results obtained in x-ray analysis are tabulated in Figure 66 where M stands for metal and O for oxide. In 1.0 Ni/Al alloys without molybdenum, a mixture of NiAl, $NiAl_3$, and Ni_3Al was found in samples A and B, where the cooling after heat treatment was through peritectic reactions. With 3% molybdenum a new phase appeared which was identified as Mo_3Al, an ordered structure with aluminum atoms at 000, ½½½, and molybdenum atoms at ¼0½, 3/4 0 ½, 0½¼, 0 ½ 3/4, 1/2 1/2 0, and 1/2 3/4 0 position (Fig. 67), and whose d and f values are calculated in the appendix. In alloys 1.0 Ni/Al and 13% molybdenum the $NiAl_3$ was not found in agreement with the increased melting point which was observed in oxidation test. As this composition corresponds to the best resistant to oxidation, the following conclusion can be established: the high melting point and resistance to oxidation for this particular composition are the results of the molybdenum added as third component which resulted in the appearance of Mo_3Al and the disappearance of $NiAl_3$ phases. The Mo_3Al phase has a **transformation at 2160°C and** the $NiAl_3$ phase has a melting point of 640°C.

In 1.5 Ni/Al alloys with 20% molybdenum, the oxide layer (B samples) was composed of $NiAl_2O_4$ and Al_2O_3. It is thought that reaction between NiO and Al_2O_3 takes place with an excess of Al_2O_3. As was shown above in Figure 27, the oxide was green-blue in color and scaled. The green-

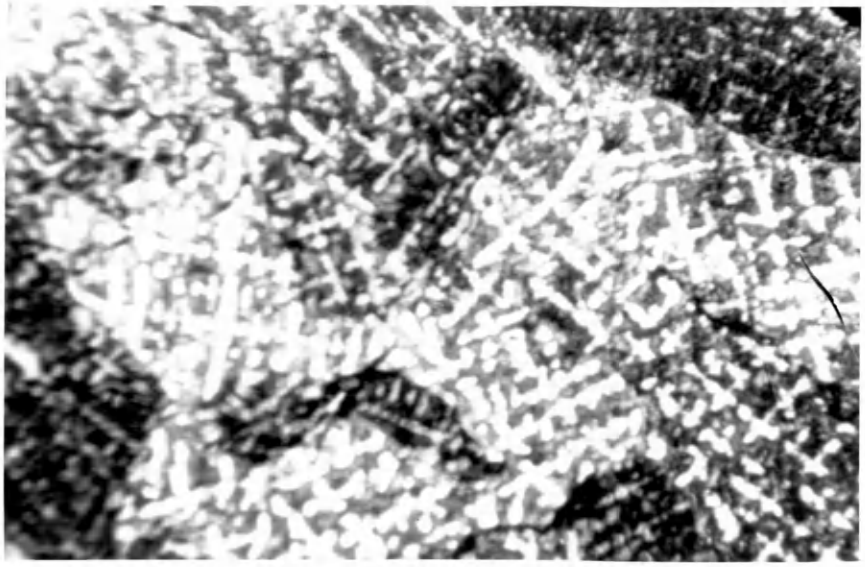

Figure 29. Ni/Al = 4.0 as cast. 700 x

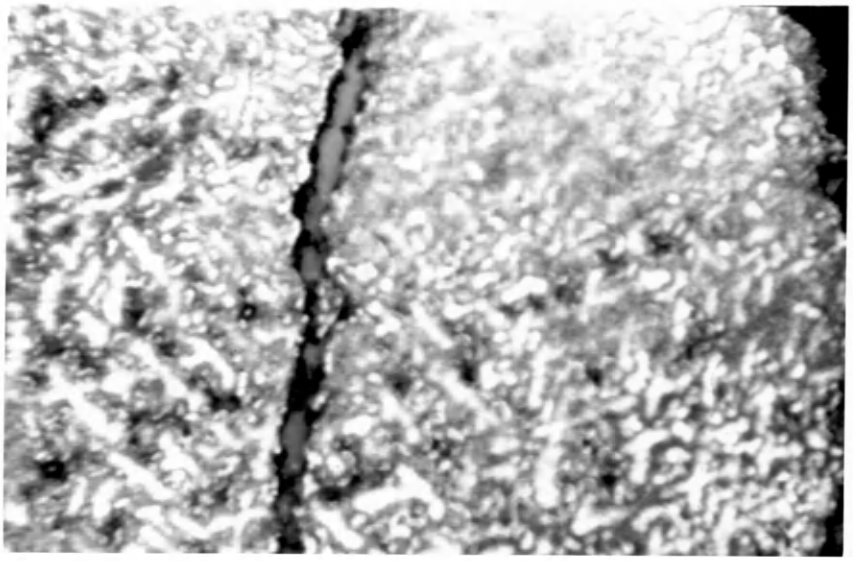

Figure 30. Ni/Al = 4.0 + 1.5% Mo as cast. 700 x

Figure 31. Ni/Al = 4.0 + 3% Mo as cast. 700 x

Figures 29-31. Oxidation tests at 1 atmosphere oxygen pressure, 1200°C and 1 minute (hot stage microscope).

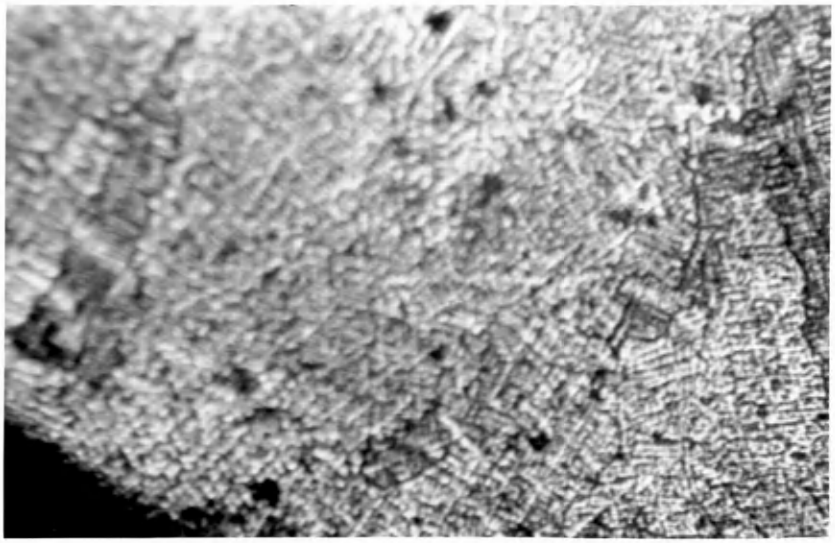

Figure 32. Ni/Al = 4.0 + 8% Mo as cast.
700 x

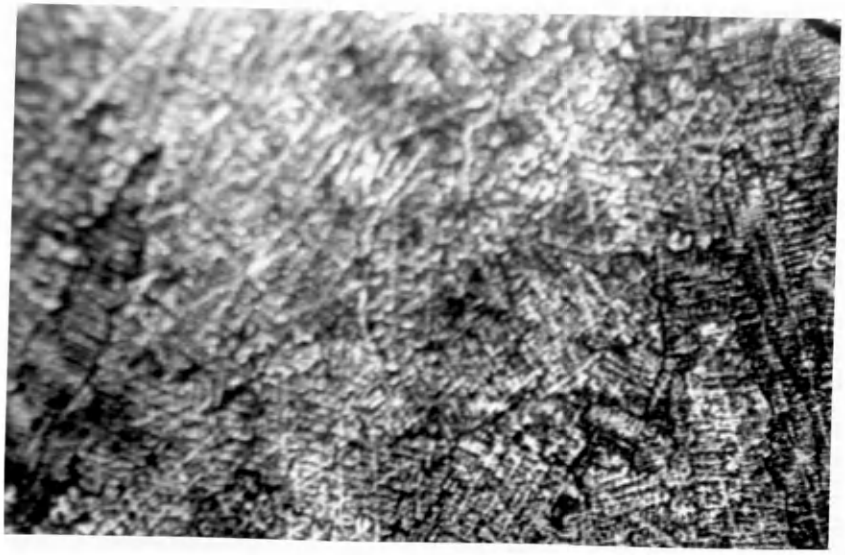

Figure 33. The same alloy after 1 minute.
700 x

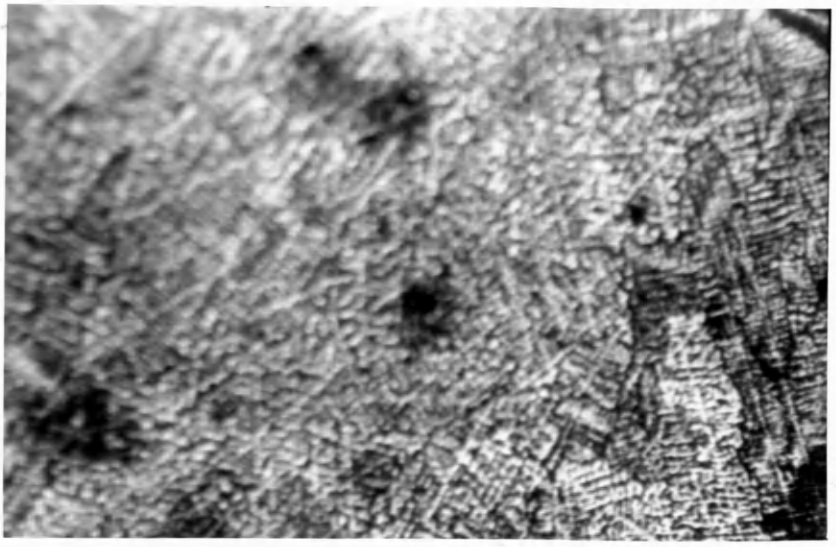

Figure 34. The same alloy after 1.5 minute. 700 x

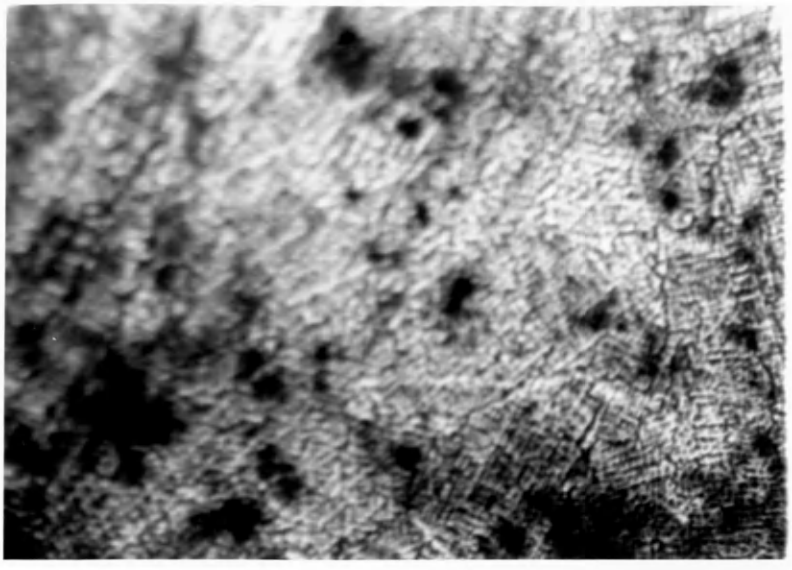

Figure 35. The same alloy after 2 minutes. 700 x

Figures 32-35. Oxidation tests at 1 atmosphere oxygen pressure, 1200°C and 0.1, 1.5, 2 minutes (hot stage microscope).

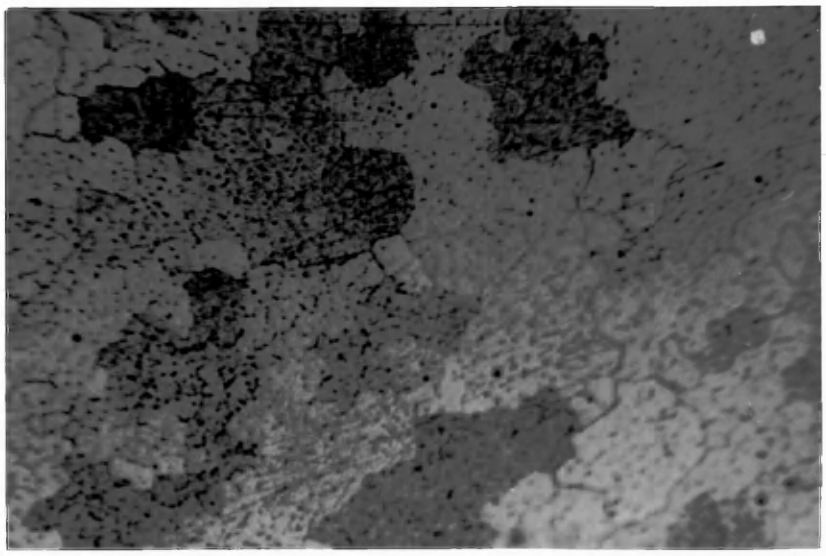

Figure 36. Ni/Al 2.3 B heat treatment.
700 x

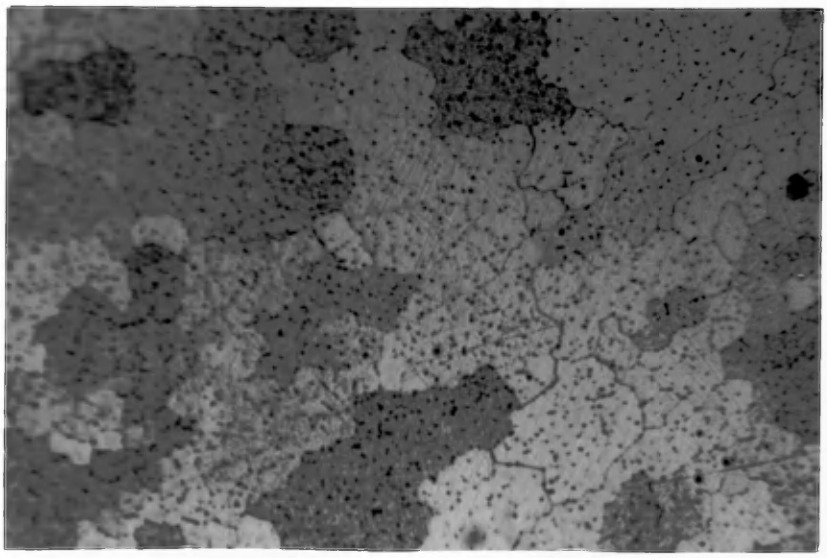

Figure 37. The same alloy after 1/2 minute.
700 x

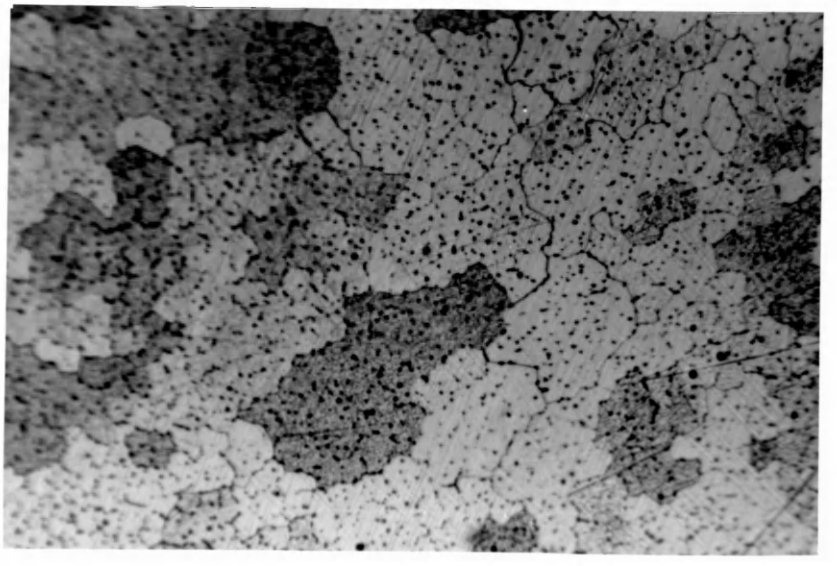

Figure 38. The same alloy after 1 minute. 700 x

Figures 36-38. Oxidation tests at 1 atmosphere oxygen pressure, 1200°C and 0, 0.5, 1 minute (hot stage microscope).

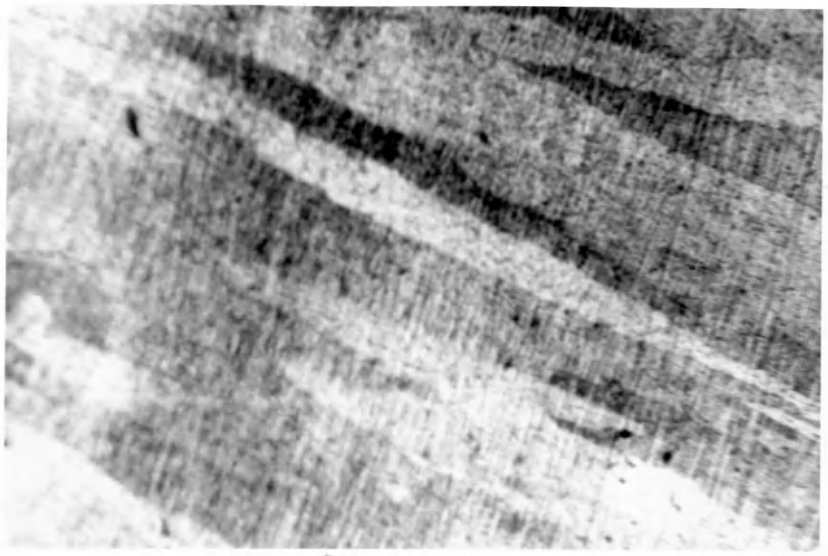

Figure 39. Ni/Al 2.3 + 3% Mo as cast.
700 x

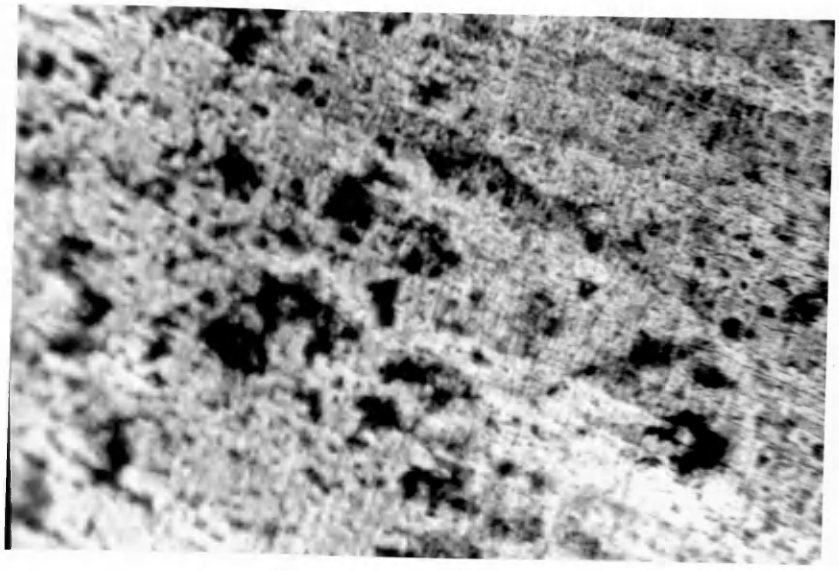

Figure 40. The same alloy after 1 minute.
700 x

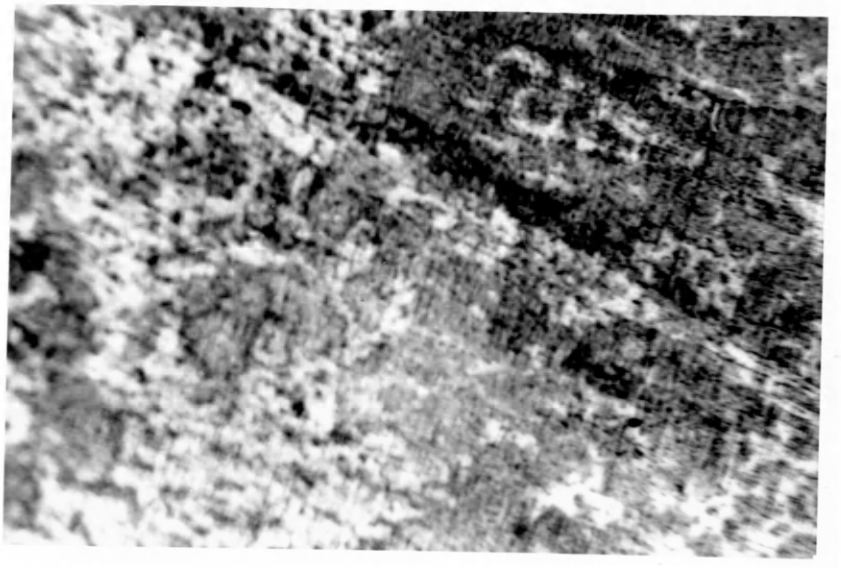

Figure 41. The same alloy after 2 minutes. 700 x

Figures 39-41. Oxidation tests at 1 atmosphere oxygen pressure, 1200°C and 0, 0.5, 2 minutes (hot stage microscope).

Figure 42. Ni/Al 2.3 + 20% Mo, B heat treatment. 700 x

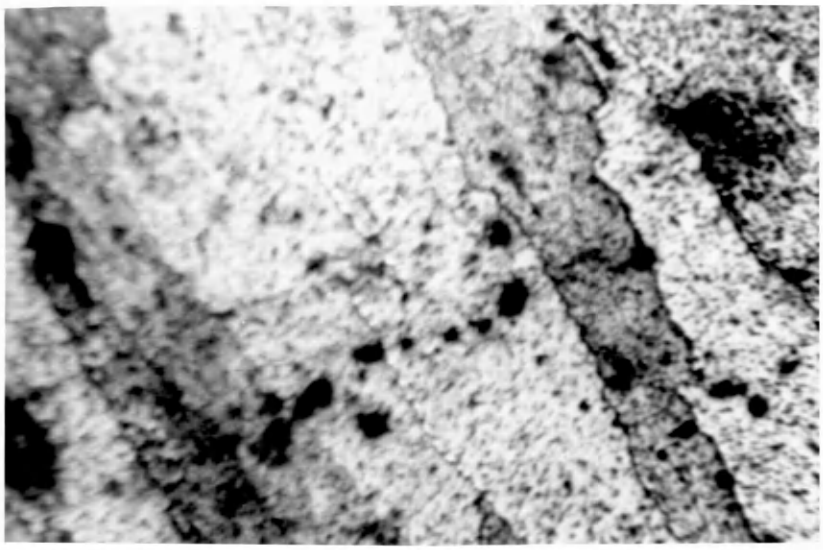

Figure 43. The same alloy after 1/2 minute. 700 x

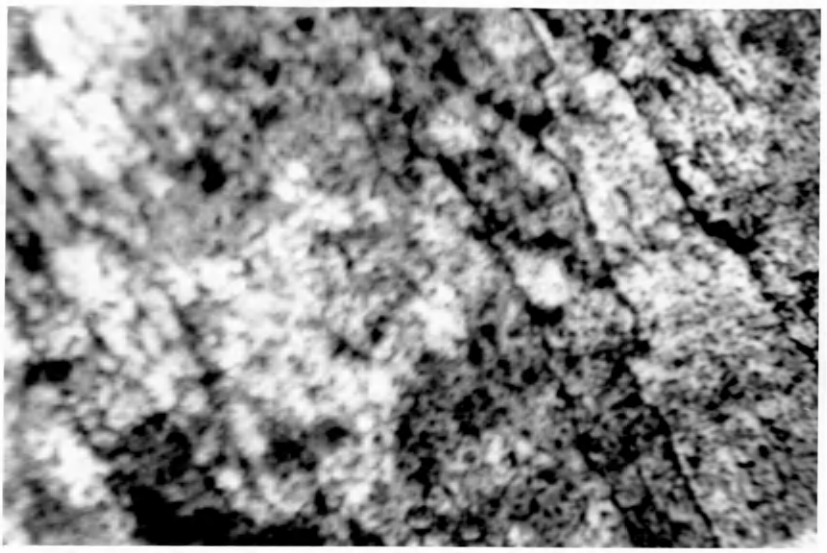

Figure 44. The same alloy after 1 minute. 700 x

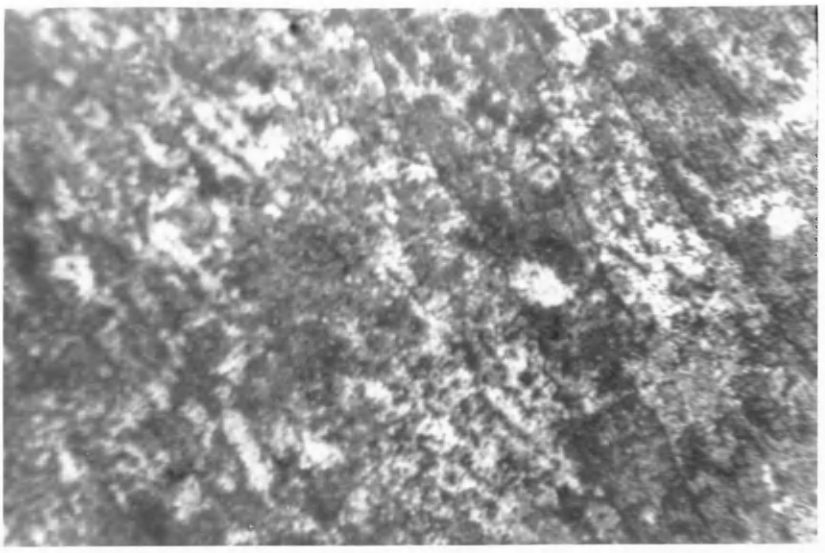

Figure 45. The same alloy after 2 minutes. 700 x

Figures 42-45. Oxidation tests at 1 atmosphere oxygen pressure, 1200°C and 0, 0.5, 1, 2 minutes (hot stage microscope).

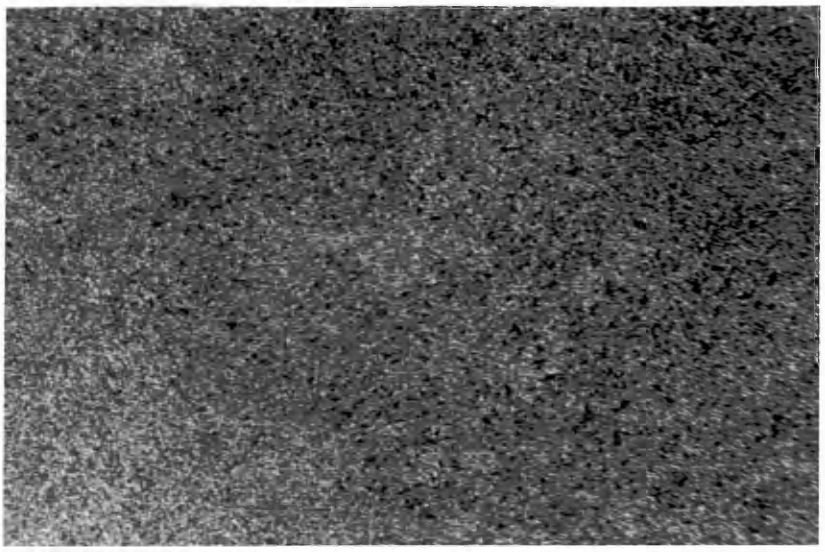

Figure 46. Ni/Al 1.5 + 3% Mo as cast.
700 x

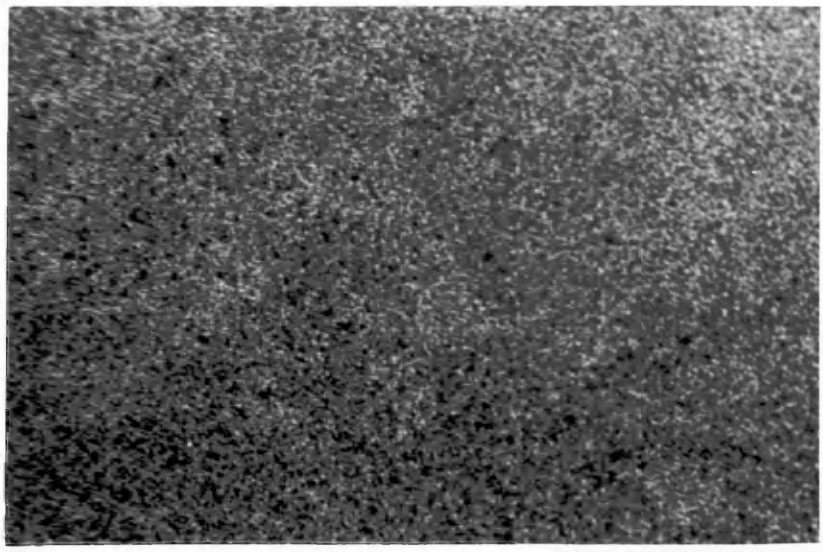

Figure 47. The same alloy. Melting begins.
700 x

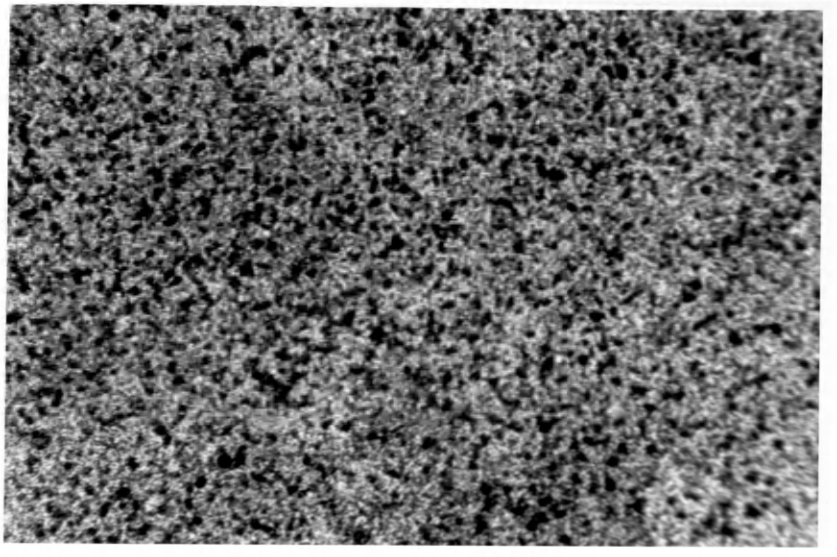

Figure 48. The same alloy. Amount of liquid increases. 700 x

Figures 46-48. Sample melted before 1200°C (hot stage microscope).

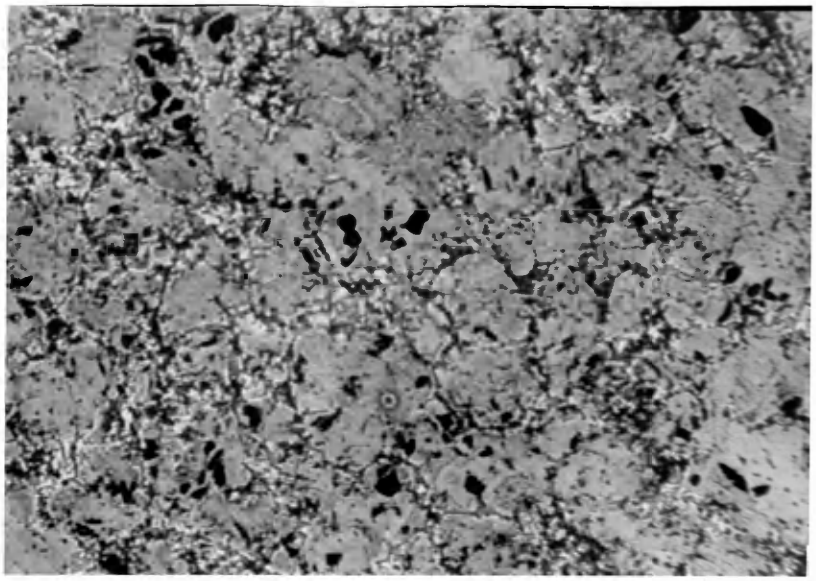

Figure 49. Ni/Al 1.0, B heat treatment.
700 x

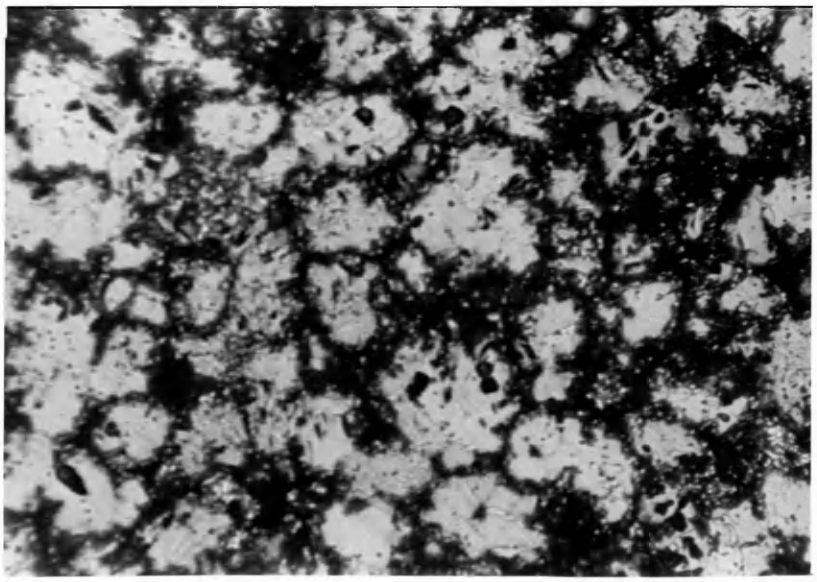

Figure 50. The same alloy. Melting starts.
700 x

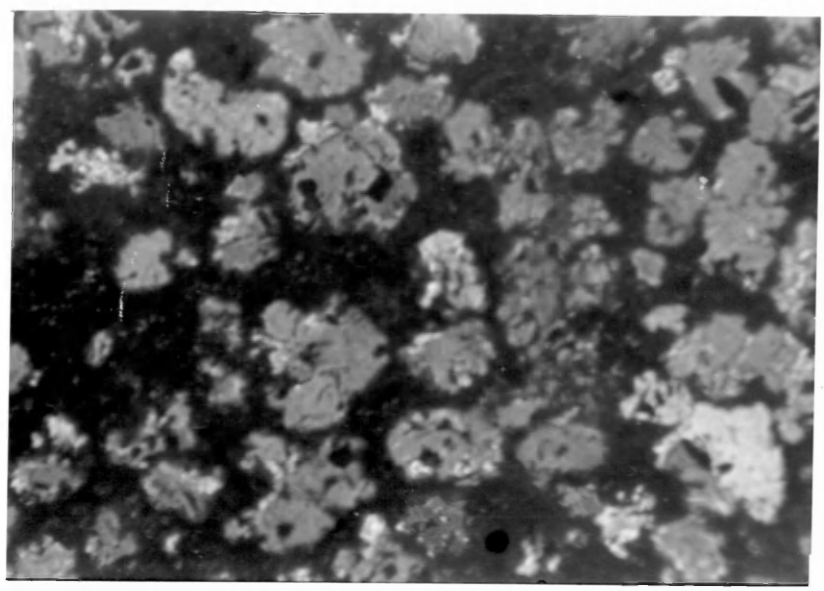

Figure 51. The same alloy. Amount of liquid increases. 700 x

Figures 49-51. Samples melted before 1200°C (hot stage microscope).

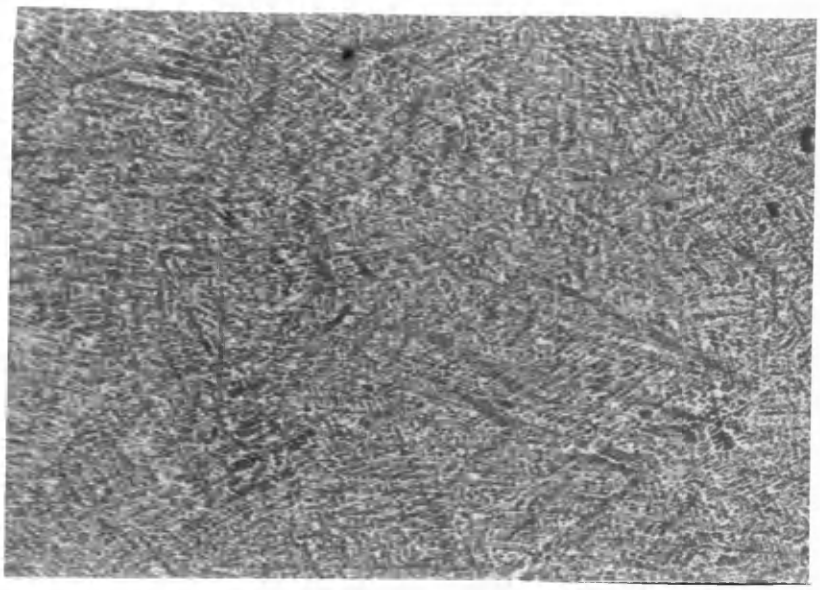

Figure 52. Ni/Al = 1 + 3% Mo as cast. 700 x

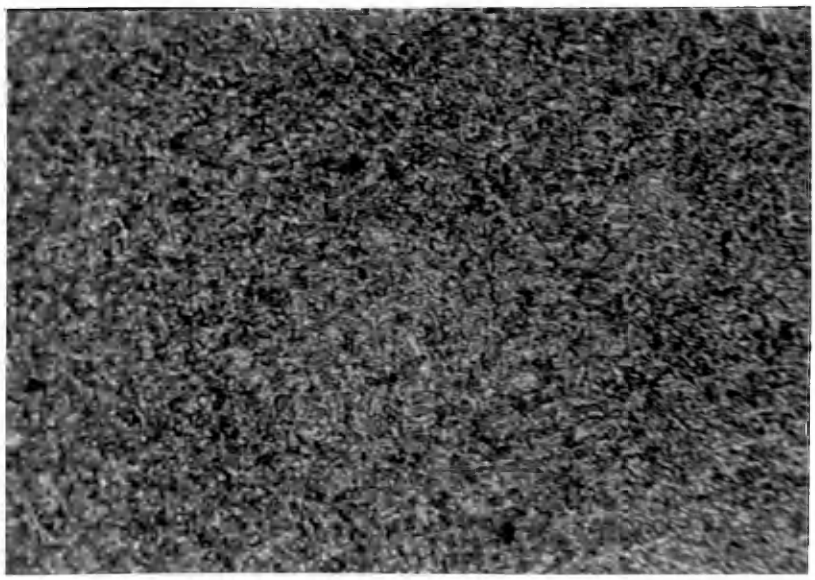

Figure 53. Same alloy after 1 minute. 700 x

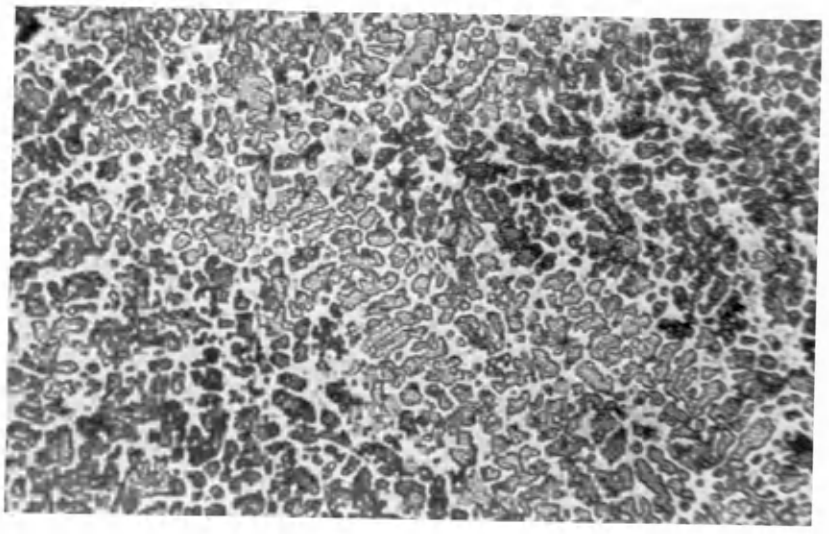

Figure 54. Same alloy, higher magnification. 2,200 x

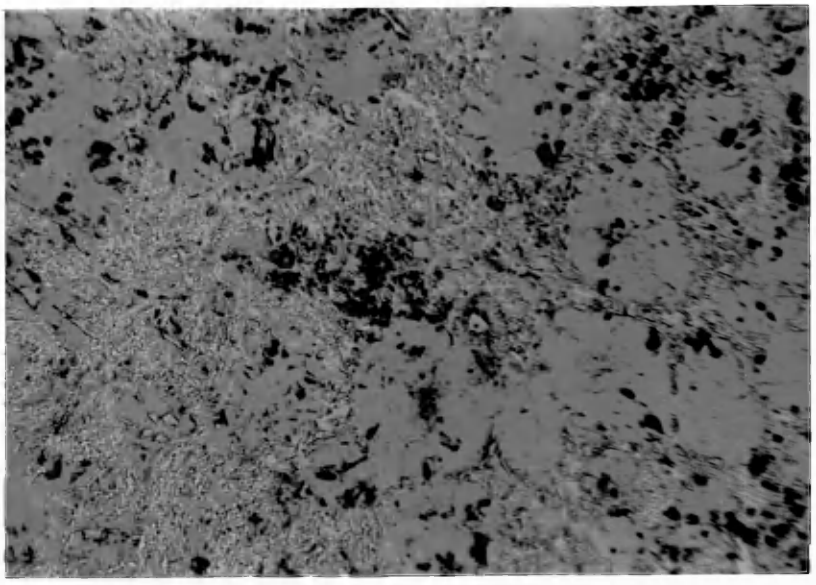

Figure 55. Ni/Al = 1 + 3% Mo, B heat treatment. 700 x, time = 0.

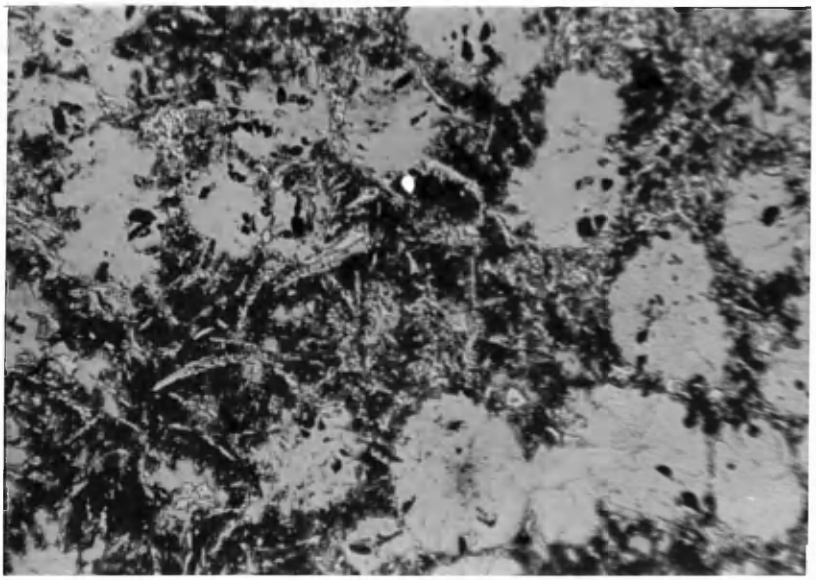

Figure 56. The same alloy. Melting starts. 700 x

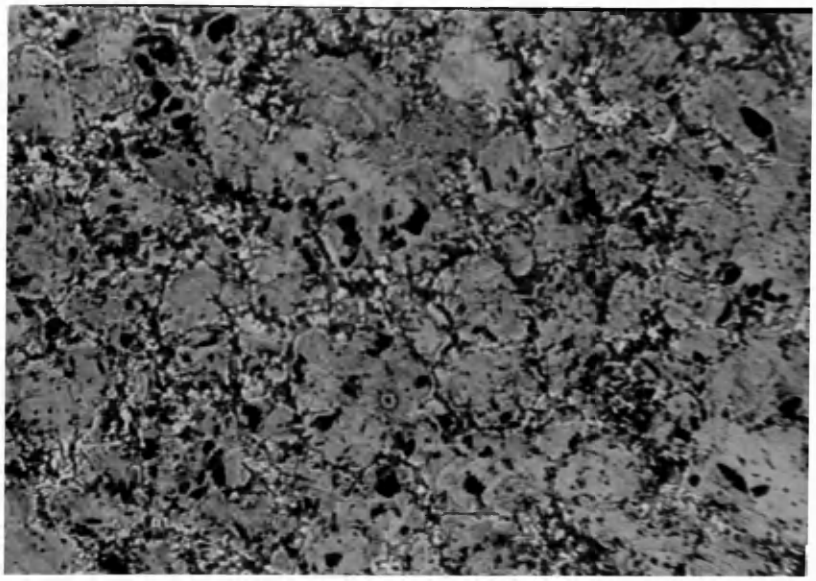

Figure 57. The same alloy. Melting proceeds. 700 x

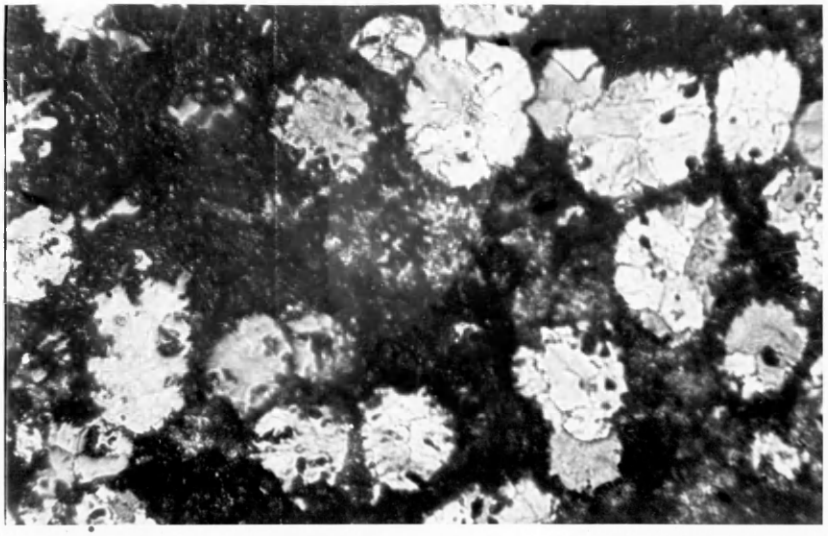

Figure 58. The same alloy. Melting proceeds. 700 x

Figures 52-58. B samples melted before 1200°C; A samples were more stable (hot stage microscope).

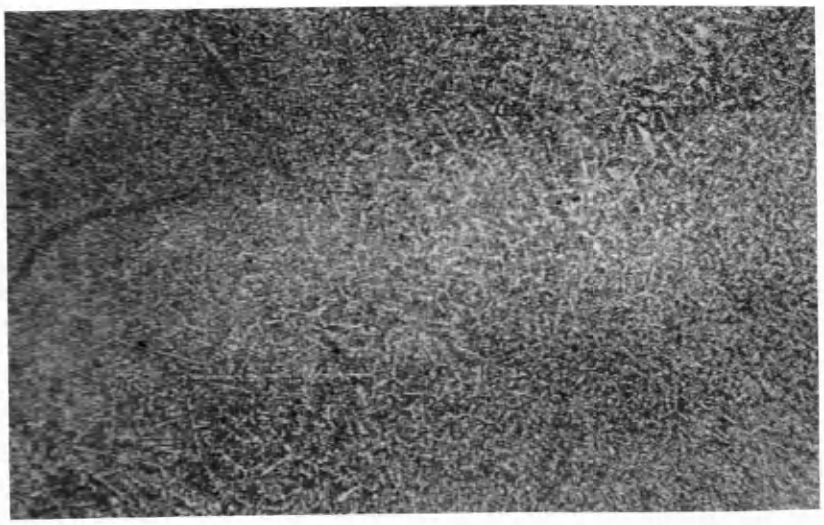

Figure 59. Ni/Al = 1 + 13% Mo as cast. 700 x

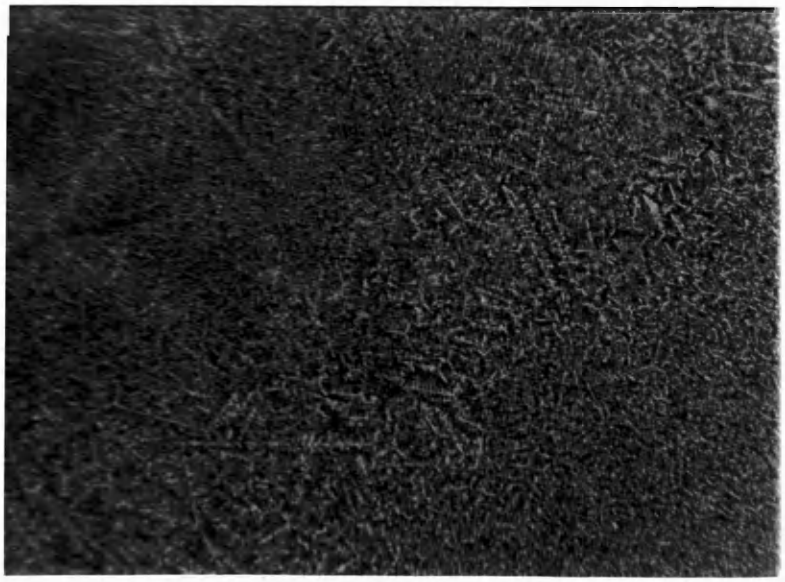

Figure 60. The same alloy after 2 minutes. 700 x

Figure 61. Same alloy, B heat treatment. 700 x

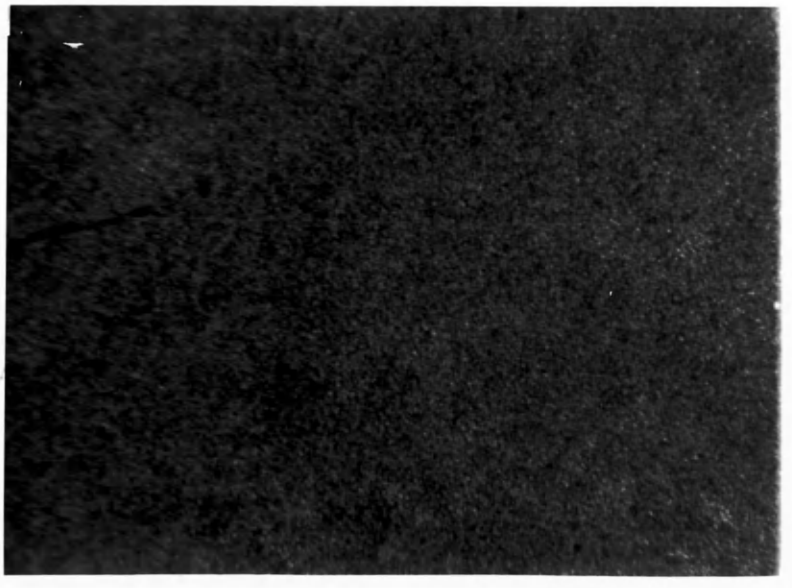

Figure 62. Same alloy after 2 minutes. 700 x

Figures 59 to 62. Oxidation test at 1 atmosphere oxygen pressure, 1200°C, and 0, 2 minutes; A and B samples (hot stage microscope).

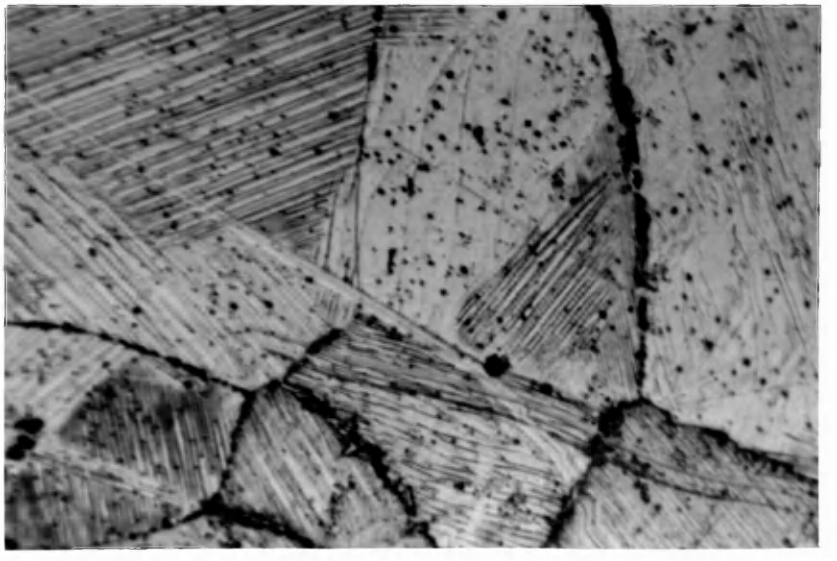

Figure 63. Ni/Al = 4 + 3% Mo, B heat treatment. 700 x

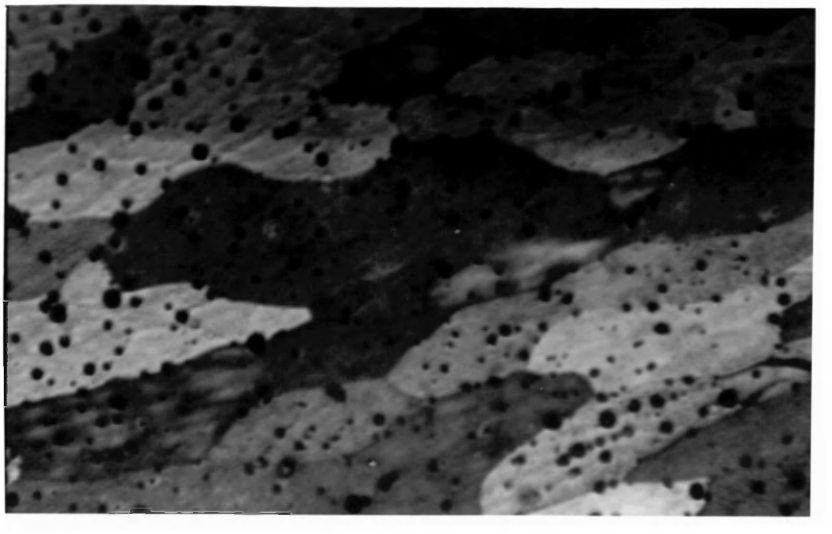

Figure 64. Ni/Al = 2.33 + 1.5 Mo, C heat treatment. 700 x

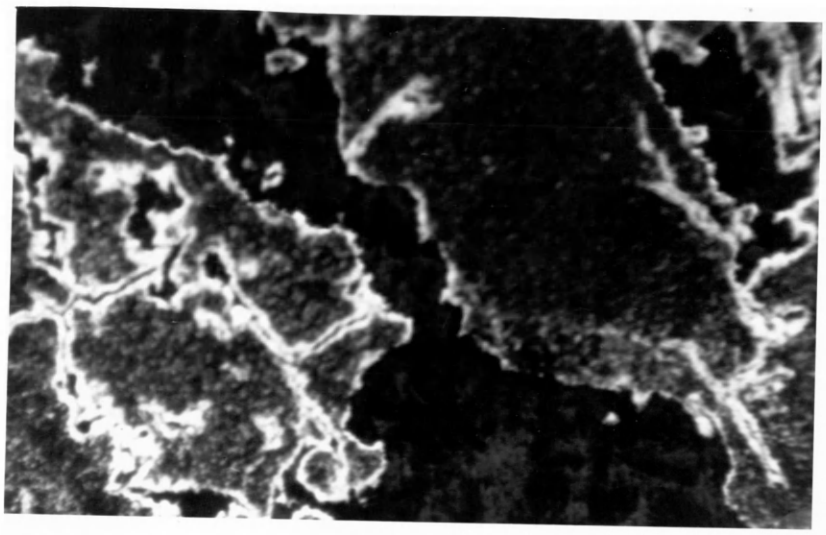

Figure 65. Ni/Al 1.5 + 3% Mo, B heat treatment, 700 x

Figures 63-65. Oxidation at oxide/metal zones (hot stage microscope).

blue color comes from the green NiO and the blue from molybdenum oxide (Kieleffer, D., 1952, p. 43) which is present in small quantity to be detected in x-rays.

Alloys with 1.5 Ni/Al and 13% or 20% molybdenum had basically the same structure as alloys with 1.0 Ni/Al and 13% molybdenum which were studied above. Therefore, the conclusions with respect to oxidation resistance are the same.

In 2.3 Ni/Al alloys with 8% molybdenum, the oxide layer in B samples was composed of $NiAl_2O_4$ and NiO and as explained above, there is a reaction between Al_2O_3 and NiO in excess. If these results are compared with those given in Figure 27, it is seen that the excess of NiO is more detrimental than the excess of Al_2O_3 because the excess of NiO produces more scaling. Piiling and Bedworth (Brophy, J. H. and others, 1966, p. 149) give the following criterion for cracking of oxides: when the ratio of the molecular volume of the oxide to the molecular volume of the metal is lower or higher than unity, the oxide layer fails by cracking. This cracking results from tensile or compressive stresses which are developed by a lack or excess of material. The molecular volume ratio for Al_2O_3/2Al is 1.28, which is almost ideal, but for NiO/Ni is 1.70, which can cause compressive stresses. Finally, the following compounds were not resolved by x-ray analysis:

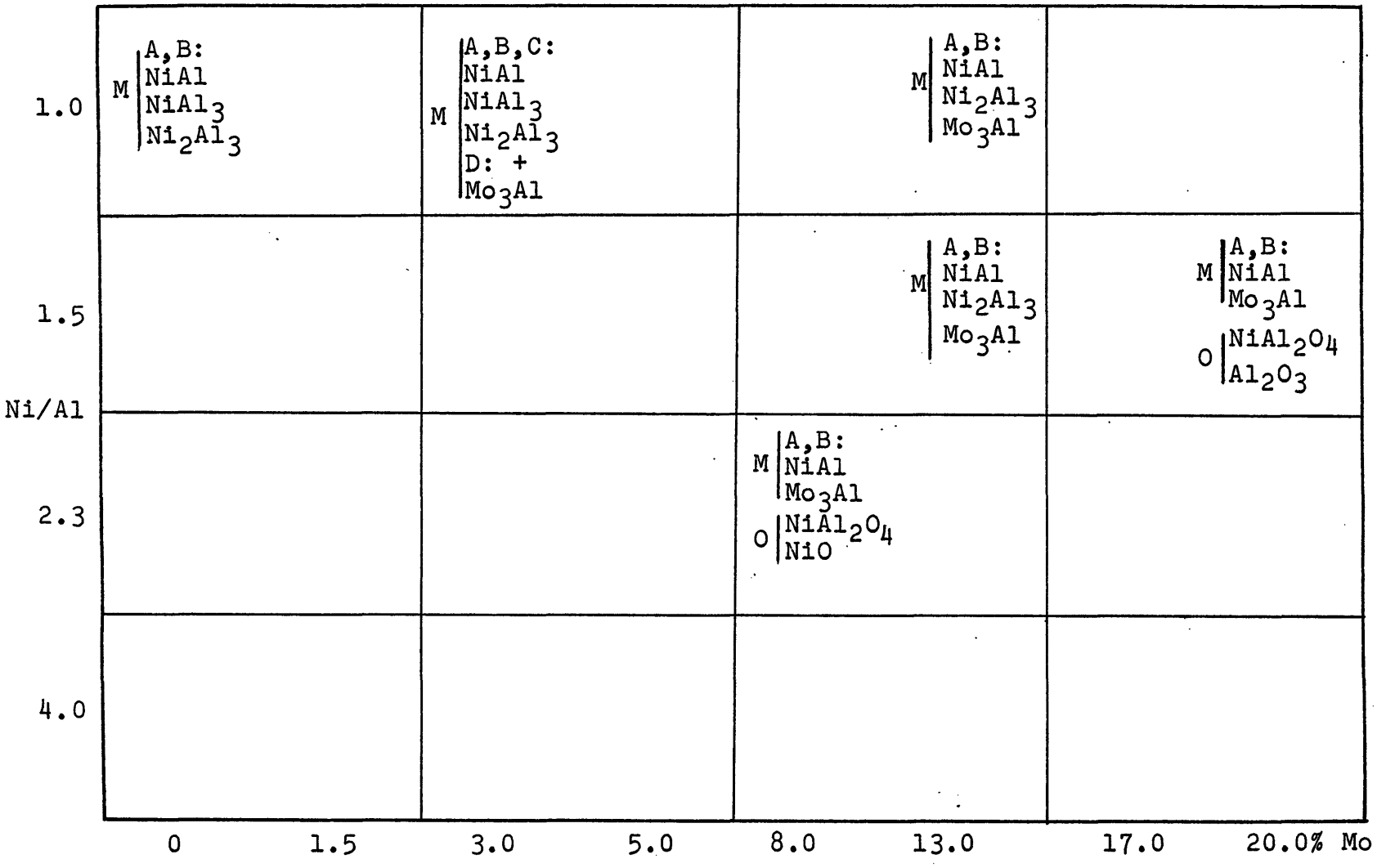

Figure 66. X-ray analysis for alloys with molybdenum up to 20%.

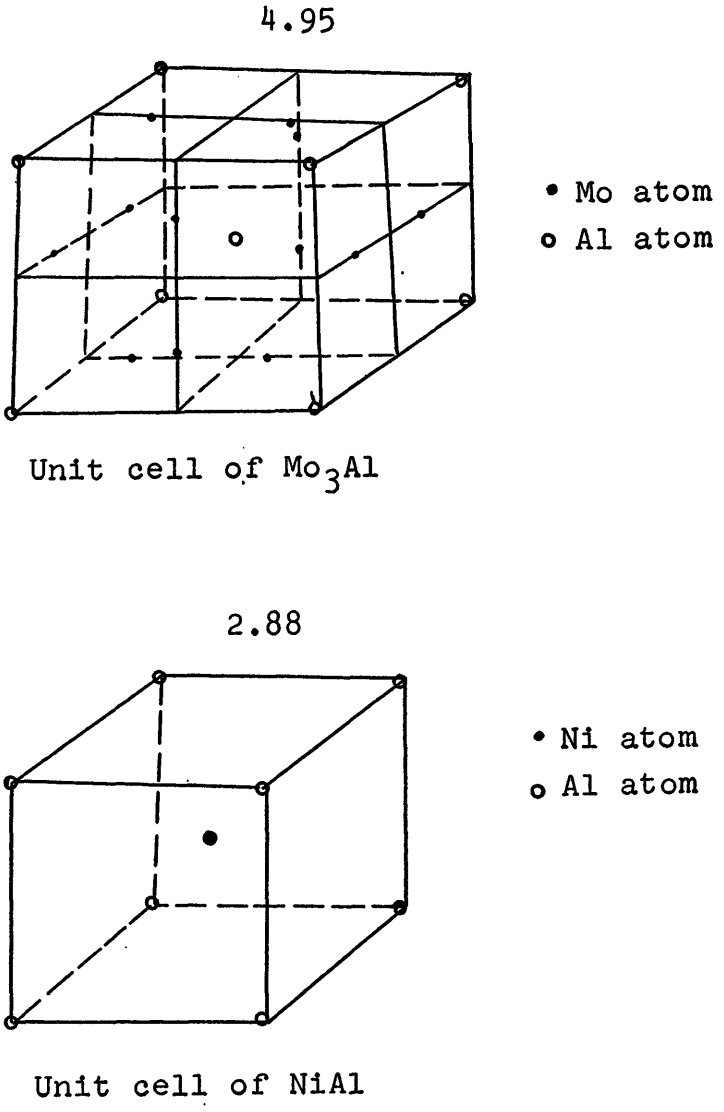

Figure 67. NiAl and Mo_3Al unit cells.

Al	not found
Ni	not found
Mo	not found
$Al_{12}Mo$	not found
Al_5Mo	lack of information
Al_3Mo	not found
Al_2Mo	lack of information
$MoNi_4$	lack of information
$MoNi_3$	lack of information
$MoNi_1$	not found
MoO_2	not found (volatilized)
MoO_3	not found (volatilized)
Mo_3Al_8	lack of information
$NiMoO_4$	not found

And some general conclusions can be given:

1. The missing $NiAl_3$ phase in some samples indicates a shift of the binary Al-Ni diagram toward the aluminum-rich side by effect of the added molybdenum. Mo_3Al phase was the only molybdenum compound found in NiAlMo alloys, but the presence of other molybdenum compounds like Al_2Mo or Mo_3Al_8 cannot be excluded (literature survey).

2. Since Al, Ni, nor Mo were not found, it can be concluded that the alloys are homogeneous in composition and that no terminal solid solutions are formed in this composition range we are working with.

3. The presence of Ni_2Al_3 in unmelted alloys at 1200°C and Ni/Al 1.0 plus 13% molybdenum in composition indicates that the melting point of this phase, which is 1150°C in binary alloys, was increased by the additions of molybdenum to above 1200°C.

4. MoO_2, MoO_3, $NiMoO_4$ were not found in agreement with the literature survey.

DISCUSSION OF EXPERIMENTAL RESULTS

Alloys with Molybdenum from 20% to 60%

As it is explained in the appendix, Table 1, Ni/Mo ratios for these alloys range from 3.2 to 0.333, Ni/Al from 1.0 to 4.0 and Al/Mo from 2.0 to 0.133. These compositions are enclosed inside the dashed areas of the figures 10, 13 and 15. Because no melting took place with any of these compositions at 1200°C, the ternary compositions do not have the low melting phases observed in binary diagrams (Al_5Mo, $NiAl_3$). Otherwise, it is increased by effect of molybdenum ($N_{12}Al_3$). In other words, the present phases do not go beyond the a' lines on AlMo and AlNi diagrams, or the melting points of Ni_2Al_3, $NiAl_3$, and the probable phases Al_3Mo, Al_5Mo and $MoAl_{12}$ was increased. High percentages of Mo caused more oxidation, perhaps because rich molybdenum compounds reacted more easily with oxygen. Unfortunately, the AlMo phase diagram has not been established for compositions lower than 40% at Al and the nature of these molybdenum compounds is unknown.

The possible effect of $MoNi_4$ and $MoNi_3$ on the oxidation of samples heat treated at 600°C cannot be explained because the NiMo phase diagram at compositions lower than 25% at Ni and below 800°C has not been established.

Alloys with Molybdenum up to 20%

As it is explained in Table 1 of the Appendix, Ni/Mo ratios for these alloys range from 52.5 to 3.2, Ni/Al from 1.0 to 4.0 and Al/Mo from 32.2 to 0.8. These compositions are enclosed between the lines M-N on NiMo and AlMo phase diagrams.

As nickel-molybdenum solid solution (Ni_α) was not found in x-ray analysis, the ternary compositions are located at the right of the line N in Figure 13, and neither $MoNi_4$ nor $MoNi_3$ will be present.

As neither Al_3Mo nor $Al_{12}Mo$ were identified in x-ray analysis, the ternary compositions are located at the right of the vertical line corresponding to the probable Al_2Mo phase and consequently no low melting lines or points will be found in regions 1.0-4.0 Ni/Al with molybdenum 0-20%.

If NiAl, MoAl, MoNi phase diagrams are observed after the above conclusions, heat treatments of 1200°C and 900°C will not change the phases of as-cast structures, but the distribution is in agreement with the results obtained in x-ray analysis which were already explained.

It has been known that aluminum rich NiAl phase oxides at slower rates than nickel rich AlNi phase (Mozhuzhin, E., and others, 1957, p. 1953). Also it was found in this research (Appendix) that small grains and conchoidal fracture took place in alloys with 1.0 Ni/Al wt, whereas large crystals and fibrous fracture occurred in alloys with 4.0 Ni/Al wt.

These facts, besides the effect of Pilling-Bedworth ratio, help to explain the difference in oxidation found with nickel content.

SUMMARY AND CONCLUSIONS

MoNiAl alloys with 1.0, 1.5, 2.3, 4.0 Ni/Al wt plus 20, 30, 40, 60% weight in molybdenum were annealed at 600°C and 1200°C, quenched in cold water and oxidized at 1200°C. The compositions more resistant to oxidation were 1.0, 1.5, 2.3, 4.0 NiAl wt plus 20% Mo. No effect of previous heat treatment on oxidation could be observed.

Based on these results, a more detailed study was performed on alloy 1.0, 1.5, 2.3, 4.0 NiAl wt plus 1.5, 3.0, 5.0, 8.0, 13.0, 17.0, 20% weight in molybdenum. The compositions most resistant to oxidation were 1.0 and 1.5 Ni/Al wt plus 13% molybdenum. Simultaneously, with this resistance to oxidation, the melting points for these alloys was increased and it is thought that some nickel-molybdenum and/or aluminum molybdenum structures are present, one of which was identified as Mo_3Al, whose melting point is 2160°C.

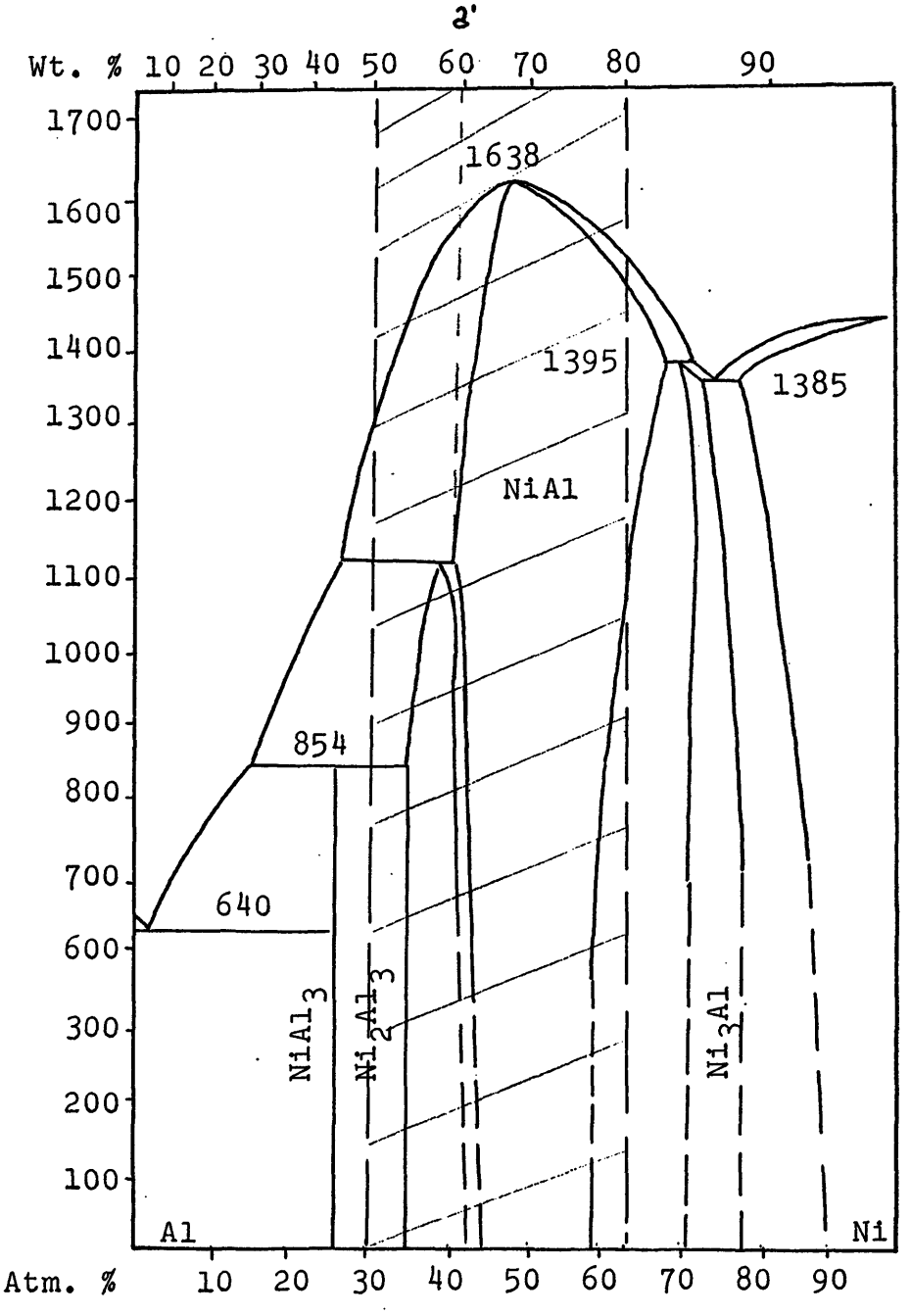

Figure 10. Al/Ni phase diagram. (From Constitution of Binary Alloys by Hansen)

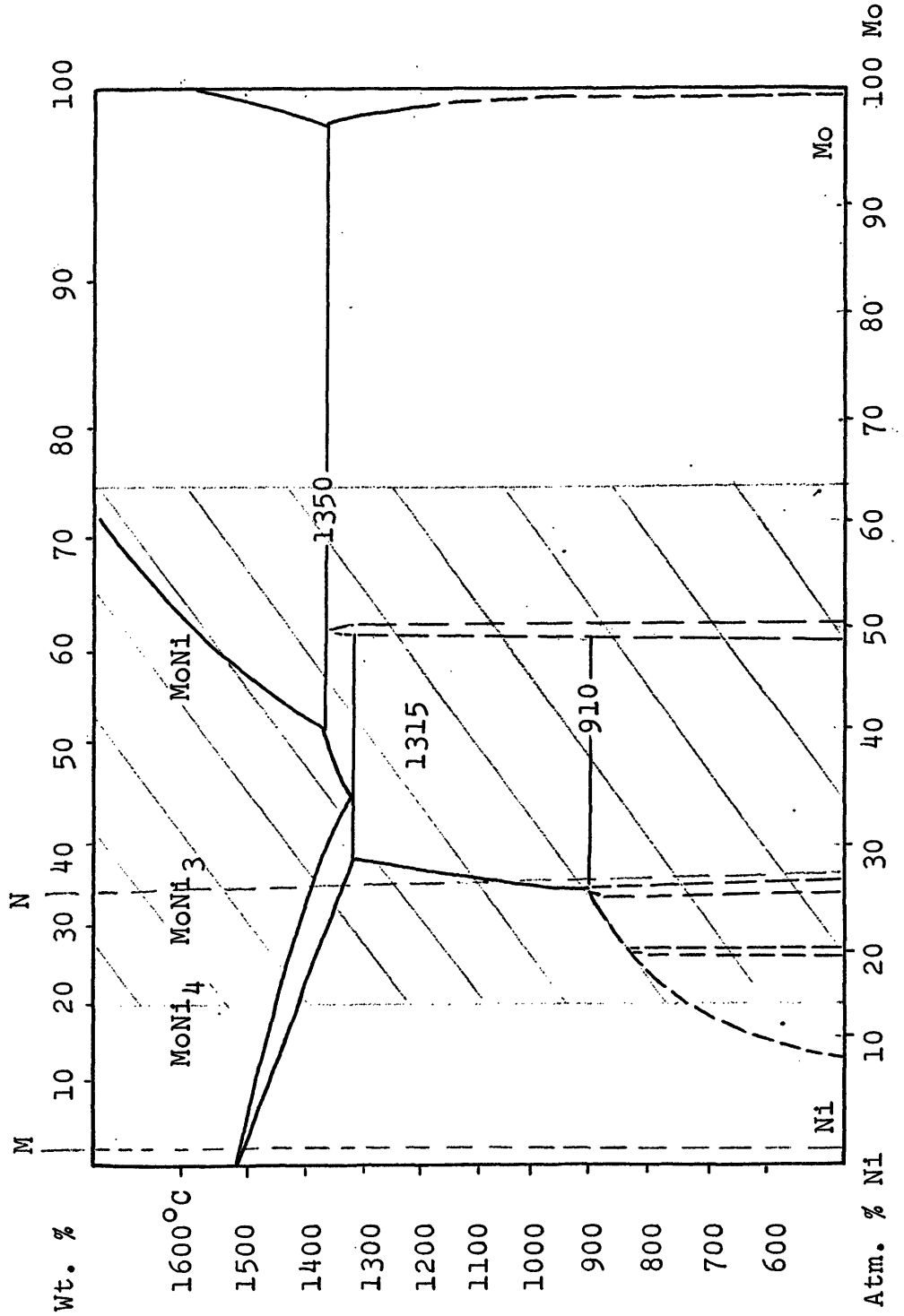

Figure 13. Ni-Mo phase diagram (From Constitution of Binary Alloys by Hansen).

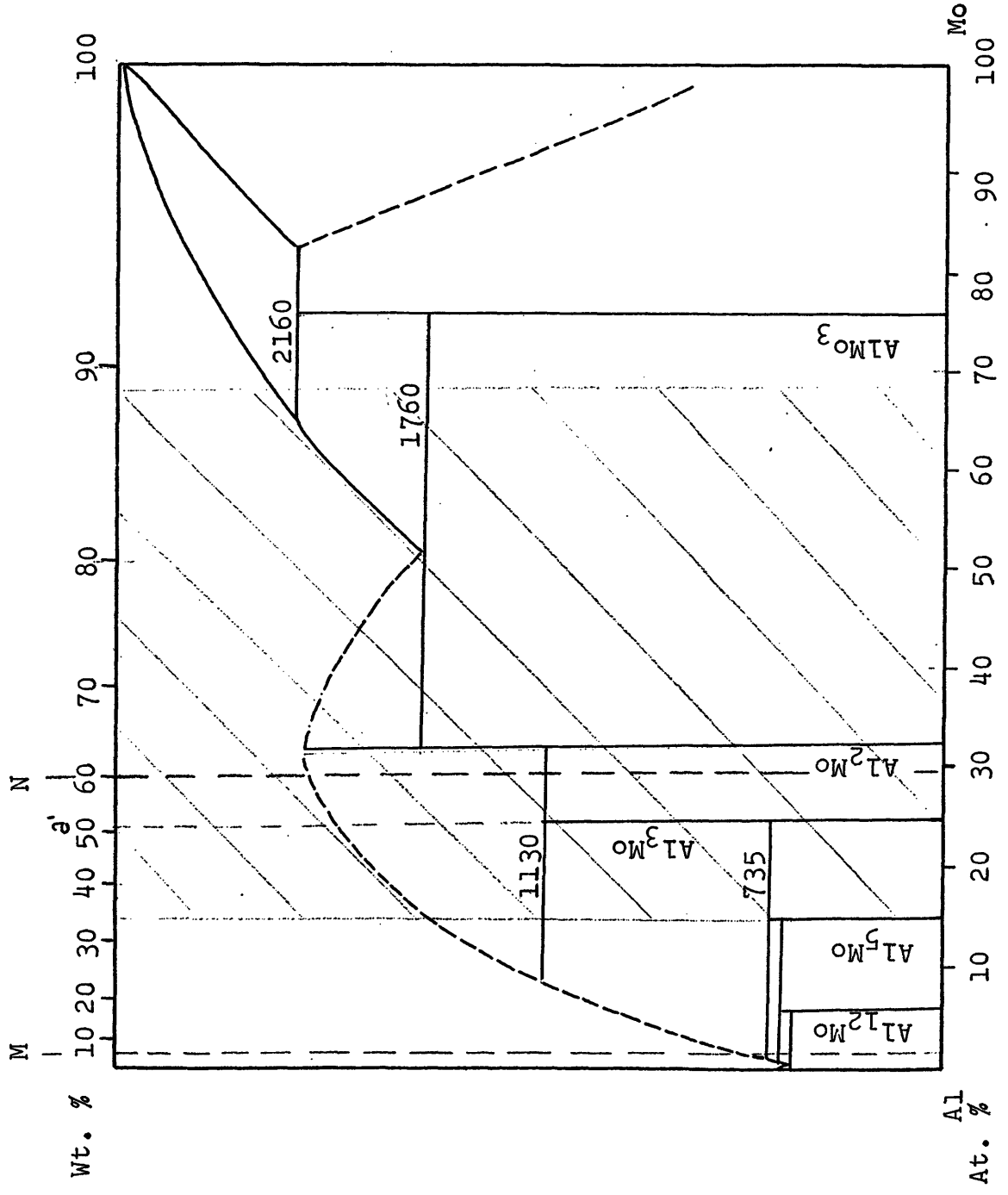

Figure 15. Al-Mo phase diagram (From Constitution of Binary Alloys by Hansen).

FURTHER STUDY

The next step to complete this research is to study the oxidation kinetics. Changes in weight with temperature at different oxygen pressures will show little because at the same time there is a gain in weight when NiO and Al_2O_3 are formed and a loss of weight when the MoO_3 is volatilized; therefore, the gravimetric study has to be accompanied by measurements in vapor pressure and gas composition at different times. Changes in composition will be checked at different positions along the oxide layer to see the variations in metal or oxygen through it, and measurements in electrical conductivities will reveal the type of predominant defect in the oxides. It will be interesting also to see the possibilities of alloys resistant to oxidation with Ni/Al less than 1.0 and high molybdenum content. It might be helpful to make a thermal analysis in order to locate melting points, especially the position of the ternary eutectic.

APPENDIX

Alloys Composition: Table 1

Alloy Number	Ni / Al	Ni / Mo	Al / Mo	Mo% wt	Ni% wt	Al% wt	Fracture, color
1	1	--	--	0	50	50	
2	1	32.8	32.8	1.5	49.25	49.25	
3	1	16.1	16.1	3.0	48.5	48.5	
4	1	9.5	9.5	5.0	47.5	47.5	
5	1	5.75	5.75	8.0	46	46	
6	1	3.4	3.4	13.0	43.5	43.5	
7	1	2.44	2.44	17.0	41.5	41.5	
8	1	2.0	2.0	20	40	40	
9	1.5	--	--	0	60	40	gray conchoidal small grains
10	1.5	39.5	26.2	1.5	59.1	39.4	
11	1.5	19.3	12.9	3.0	58.2	38.8	
12	1.5	11.4	7.6	5.0	57	38	
13	1.5	6.9	4.6	8.0	55.2	36.8	
14	1.5	4.0	2.7	13.0	52.2	34.8	
15	1.5	2.94	1.95	17.0	49.8	33.2	
16	1.5	2.40	1.6	20	48	32	
17	2.3	--	--	0	70	30	gray-green crystalline medium-sized grains
18	2.3	46	20	1.5	68.95	29.6	
19	2.3	22.5	97	3.0	67.9	29.1	
20	2.3	13.3	5.7	5.0	66.5	28.5	
21	2.3	8	3.46	8.0	64.4	27.6	
22	2.3	4.66	2	13.0	60.9	26.1	
23	2.3	3.42	1.46	17.0	58.1	24.9	
24	2.3	2.8	1.2	20	56	24	
25	4.0	--	--	0	80	20	bright crystalline large grains
26	4.0	52.5	13.1	1.5	78.8	19.7	
27	4.0	25.6	6.5	3.0	77.6	19.4	
28	4.0	15.2	3.8	5.0	76.0	19.0	
29	4.0	9.2	2.3	8.0	73.6	18.4	
30	4.0	5.35	1.34	13.0	69.6	17.4	
31	4.0	3.9	0.98	17.0	66.4	16.6	
32	4.0	3.2	0.8	20	64	16	
33	1	2	2	20	40	40	
34	1	1.16	1.16	30	35	35	
35	1	0.75	0.75	40	30	30	
36	1	0.333	0.33	60	20	20	
37	1.5	2.4	1.6	70	48	32	
38	1.5	1.4	0.93	30	42	28	
39	1.5	0.9	0.67	40	36	24	
40	1.5	0.4	0.268	60	24	16	
41	2.3	2.8	1.2	20	56	24	

Table 1 (Cont.)

Alloy Number	$\frac{Ni}{Al}$	$\frac{Ni}{Mo}$	$\frac{Al}{Mo}$	Mo% wt	Ni% wt	Al% wt
42	2.3	1.6	0.7	30	49	21
43	2.3	1.05	0.45	40	42	18
44	2.3	0.47	0.2	60	28	12
45	4.0	3.2	0.8	20	64	16
46	4.0	1.86	0.47	30	56	14
47	4.0	1.2	0.3	40	48	12
48	4.0	0.53	0.133	60	32	8

X-ray Calculations for Mo_3Al Solid Phase

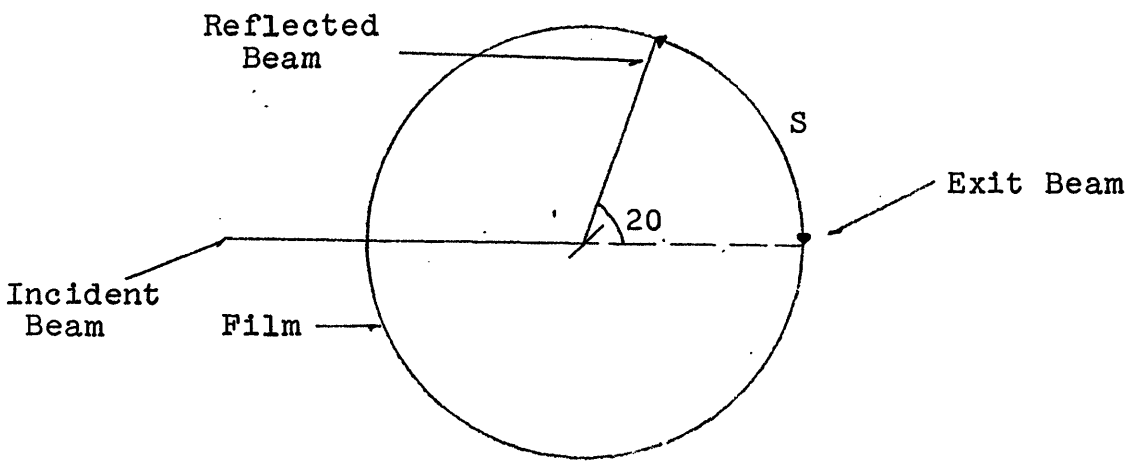

a) The diffraction angle θ, associated with each line in the pattern can be carried out using the adjacent figure:

$$\theta = \frac{s}{2r} = 0.1s \text{ radians}$$

$$\theta = \frac{s}{2r}\frac{360}{2\pi} = 5.728s \text{ degrees}$$

where:

s = one-half the distance between two areas of the reflected radiation

r = radius of the camera: 5 cm

b) The d lines are calculated applying Bragg's equation:

$$d = \frac{1.54}{2\sin\theta} = \frac{0.77}{\sin 5.728s}$$

$$d = \frac{a}{h^2+k^2+L^2} = \frac{4.95}{h^2+k^2+L^2} \quad \text{(cubic structure)}$$

where:

d = interplanar distance

a = lattice parameter which is 4.95 (Hansen, M., and Anderko, K., p. 117).

The following results were obtained:

Planes	s distance	d distance	Observed Relative Intensity
100	1.56 cm	4.95 Å	0
110	2.21 cm	3.52 "	50
111	2.83 cm	2.88 "	0
200	3.22 cm	2.47 "	75
210	3.55 cm	2.21 "	100
211	3.94 cm	2.02 "	75

c) The intensity of the beam diffracted by the atoms of the unit cell in a direction predicted by the Bragg's law is proportional to $|F|^2$, where F is the structure factor that is the resistant wave scattered by the atoms in that direction. The Mo_3Al has a cubic lattice with 2 aluminum atoms and 6 molybdenum atoms per unit cell located in the following positions (Ham, J. and Herzig, A., p. 727-728; and Wycroft, R.).

Al: 000, 1/2 1/2 1/2

Mo: 1/4 0 1/2
3/4 0 1/2
0 1/2 1/4
0 1/2 3/4
1/2 1/4 0
1/2 3/4 0

and F will be the sum of all atomic scattering factors for each atom

$$F = f_{Al}(e^{2\pi i(0)} + e^{\pi i(h+k+l)} + f_{Mo}(e^{\pi i(h/2+l)} + e^{\pi i(3h/2+l)}$$

$$+ e^{\pi i(k+l/2)} + e^{\pi i(k+3h/2)} + e^{\pi i(h+k/2)} + e^{\pi i(h+3k/2)}$$

Applying this equation to planes 100, 110, 111, 200, 210, and 211 we will have their respective relative intensity:

Plane 100

$$F_{100} = f_{Al(0)} + f_{Mo}(\cos\frac{\pi}{2} + i\sin\frac{\pi}{2} + \cos\frac{3\pi}{2}$$

$$F_{100} = f_{Mo}(0 + i + 0 - i)$$

$$F_{100} = 0$$

$|F_{100}|^2 = 0$ $\therefore$ No diffraction.

Plane 110

$$F_{110} = 2f_{Al} + f_{Mo}(e^{\frac{\pi i}{2}} + e^{\frac{3\pi i}{2}} - 1 - 1 + e^{\frac{3\pi i}{2}} + e^{\frac{5\pi i}{2}}$$

$$F_{110} = 2f_{Al} + f_{Mo}(\cos\frac{\pi}{2} + i\sin\frac{\pi}{2} + 2\cos\frac{3\pi}{2}$$

$$+ 2i\sin\frac{3\pi}{2} + \cos\frac{5\pi}{2} + i\sin\frac{5\pi i}{2} - 2)$$

$$F_{110} = 2f_{Al} + f_{Mo}(0 + i + 0 - 2i + 0 + i - 2)$$

$$F_{110} = 2(f_{Al} - f_{Mo})$$

$|F_{110}|^2 = 4(f_{Al} - f_{Mo})^2$ $\therefore$ diffraction

Plane 111

$$F_{111} = f_{Mo}(3e^{\frac{3\pi i}{2}} + 3e^{\frac{5\pi i}{2}}$$

$$F_{111} = 3f_{Mo}(\cos\frac{3\pi}{2} + i\sin\frac{3\pi}{2} + \cos\frac{5\pi}{2} + i\sin\frac{5\pi}{2})$$

$$F_{111} = 3f_{Mo}(0 - i + 0 + i)$$

$$F = 0$$

$$|F|^2 = 0 \qquad \therefore \text{ no diffraction}$$

Plane 200

$$F = 2f_{Al} + f_{Mo}(e^{\pi i} + e^{3\pi i} + 2 + e^{2\pi i} + e^{2\pi i})$$

$$F = 2(f_{Al} + f_{Mo})$$

$$|F|^2 = 4(f_{Al} + f_{Mo})^2 \qquad \therefore \text{ diffraction}$$

Plane 210

$$F = f_{Mo}(e^{\pi i} + e^{3\pi i} + e^{\pi i} + e^{\pi i} + e^{5\pi i/2} + e^{7\pi/2}$$

$$F = (\cos \frac{5\pi}{2} + i \sin \frac{5\pi}{2} + \cos \frac{7\pi}{2} + i \sin \frac{7\pi}{2} - 4)$$

$$F = f_{Mo}(0 + i + 0 - i - 4)$$

$$|F|^2 = 16 f_{Mo}^2 \qquad \therefore \text{ diffraction}$$

Plane 211

$$F = 2f_{Al} + f_{Mo}(e^{2\pi i} + e^{4\pi i} + e^{\frac{3\pi i}{2}} + e^{\frac{5\pi i}{2}} + e^{\frac{5\pi i}{2}} + e^{\frac{7\pi i}{2}})$$

$$F = 2f_{Al} + f_{Mo}(2 + \cos \frac{3\pi}{2} + i \sin \frac{3\pi}{2} + 2 \cos \frac{5\pi}{2}$$

$$+ 2 i \sin \frac{5\pi}{2} + \cos \frac{7\pi}{2} + i \sin \frac{7\pi}{2})$$

$$F = 2(f_{Al} + f_{Mo})$$

$$F^2 = 4(f_{Al} + f_{Mo})^2 \qquad \therefore \text{ diffraction}$$

Thermodynamics in Aluminum Oxide Formation at 1200°C

The oxidation reaction is

$$2Al + \frac{3}{2} O_2 \rightarrow Al_2O_3$$

The free energy change associated with the reaction at 1200°C is: 285.000 cal/g.mole (Wicks, C., and Block, F., 1963, p. 13).

Because $\Delta F_T = -RT/nk$

at 1200°C

$$k = \frac{285.000}{-1.97 \times 2.3 \times 1473} \log^{-1} \text{ (equilibrium constant)}$$

$$k = 10^{-40}$$

but

$$k = (P_{O_2})^{3/2}$$

and

$$\therefore \quad P^i_{O_2} = 10^{-28} \text{ atmospheres}$$

Thermodynamics in Nickel Oxide Formation

The oxidation reaction is:

$$Ni + \tfrac{1}{2}O_2 \rightarrow NiO$$

The free energy change associated with the reaction is given by Wicks, C., and Block, F. (1963, p. 86) as:

$$\Delta F_T = 21.590 - 0.12\ T\ln T + 0.04 \times 10^{-3}\ T^2$$

$$- 0.03 \times 10^{5} T^{-1}\ 22T$$

where T is given in Kelvin degrees.

Because $\Delta F_T = -RT\ln k$ at 1200°C

$$k = \frac{27.000}{-1.97 \times 2.3 \times 1473} \log^{-1} \quad \text{(equilibrium constant)}$$

$$k = 1.2 \times 10^{-4}$$

but as $k = (P^{o}_{O_2})^{\frac{1}{2}}$ in dissociation

then: $P^{i}_{O_2} = 1.1 \times 10^{-8}$ atmospheres

As a consequence, still little oxygen pressure is needed to start the oxidation in nickel, but it is more resistant than aluminum.

BIBLIOGRAPHY

Alexsandrovich, N., and Pavlovich, V., 1966, High temperature chemistry of silicates and other systems: New York, Consultants Bur., 216 p.

Azou, P., 1966, Diagrams d'equilibre: Paris, 21 rue Cassete, 50 p.

Bradley, A. J., 1937, Royal Soc. Proc., v. 82, p. 56-72.

Brophy, J. H., 1966, Thermodynamics of structure: New York, John Wiley, 216 p.

Burns, R., and De Maria, J., 1960, Jour. Chem. Phys., v. 82, p. 1363.

Elliot, R. P., 1965, Constitution of binary alloys, first supplement: New York, McGraw-Hill, 980 p.

Farnsworth, H., and Tuul, J., 1958, Phys. Chem. Solids, v. 1, p. 48.

Guy, A. G., 1960, Elements of physical metallurgy: New York, Addison-Wesley Co., 527 p.

Ham, J., and Herzing, A., 1950, Am. Soc. Mech. Eng. Trans., v. 73, p. 727-728.

Hansen, M., and Anderko, K., 1958, Constitution of binary alloys: New York, McGraw-Hill, 1305 p.

Haufle, K., 1965, Oxidation of metals: New York, Plenum Press, 541 p.

Keeffe, M., and Moore, W., 1961, Jour. Phys. Chem., v. 65, p. 1438.

Kelly, K., 1935, Bur. Mines Bull., 383, 140 p.

Killeffer, D. H., 1952, Molybdenum compounds: New York, Interscience Publishers, 407 p.

Kofstad, P., 1966, High temperature oxidation of metals: New York, John Wiley, 340 p.

Kubaschewski, O., and Hopkins, B., 1953, Oxidation of metals and alloys: London, Academic Press, 239 p.

Mozhuzhin, L., and others, 1957, Jour. Appl. Chem., (USSR) v. 30, p. 1543.

Oishi, Y., 1957, Jour. Chem. Phys., v. 26, p. 182.

Paladino, A., 1962, Jour. Chem. Phys., v. 37, p. 457.

Shunk, F. A., 1969, Constitution of binary alloys, second supp.: New York, McGraw-Hill, 720 p.

Sitzer, D., 1964, Met Progr., v. 85, p. 86.

Smithells, C., and others, 1928, Jour. Inst. Met., v. 40, p. 269.

Taylor, A., and Brenda, J., 1962, Crystallographic data on metals and alloy structures: New York, Dover Publications, 263 p.

Vicks, C., and Block, F., 1963, U.S. Bur. Mines Bull. 605, 146 p.

Wycroft, R., 1960, Crystal structures: New York, Interscience Publishers, v. 7, 250 p.